

1 **Quantifying the contributions of atmospheric processes and meteorology to severe**
2 **PM_{2.5} pollution episodes during the COVID-19 lockdown in the Beijing-Tianjin-**
3 **Hebei, China**

4 Ishaq Dimeji Sulaymon^a, Yuanxun Zhang^{b,c}, Philip K. Hopke^{d,e}, Song Guo^f, Fei Ye^a, Jinjin
5 Sun^a, Yanhong Zhu^a, Jianlin Hu^{a*}

6
7 ^a Jiangsu Key Laboratory of Atmospheric Environment Monitoring and Pollution Control,
8 Collaborative Innovation Center of Atmospheric Environment and Equipment Technology,
9 School of Environmental Science and Engineering, Nanjing University of Information
10 Science and Technology, Nanjing, 210044, China

11 ^b College of Resources and Environment, University of Chinese Academy of Sciences,
12 Beijing 100049, China

13 ^c CAS Center for Excellence in Regional Atmospheric Environment, Chinese Academy of
14 Sciences, Xiamen, 361021, China

15 ^d Center for Air Resources Engineering and Science, Clarkson University, Potsdam, NY
16 13699, USA

17 ^e Department of Public Health Sciences, University of Rochester School of Medicine and
18 Dentistry, Rochester, NY 14642, USA

19 ^f State Key Joint Laboratory of Environmental Simulation and Pollution Control, College
20 of Environmental Sciences and Engineering, Peking University, Beijing, 100871, China

21 _____
22 * Corresponding author. E-mail address: sulaymondimeji@nuist.edu.cn; jianlinhu@nuist.edu.cn

23
24 **Key Points:**

- 25 • Three severe PM_{2.5} pollution episodes were identified in the Beijing-Tianjin-Hebei
26 region during the COVID-19 lockdown.
27
28 • The PM_{2.5} episodes were dominated by emissions and aerosol processes, and
29 enhanced by unfavorable meteorological conditions.
30
31 • Designing more effective emissions control strategies with both chemistry and
32 meteorology in thought could mitigate future PM_{2.5} episodes.
33

34 **Abstract**

35 A major tool for curtailing the spread of COVID-19 pandemic in China was a
36 nationwide lockdown, which led to significant reductions in anthropogenic emissions and
37 fine particulate matter (PM_{2.5}). However, the lockdown measures did not prevent high
38 PM_{2.5} pollution episodes (EPs). Three severe EPs were identified in the Beijing-Tianjin-
39 Hebei (BTH) region during the lockdown. The integrated process rate (IPR) analysis tool
40 in the Community Multiscale Air Quality (CMAQ) model was employed to quantify the
41 contributions of individual atmospheric processes to PM_{2.5} formation during the lockdown
42 in the BTH region. The IPR results showed that emissions and aerosol processes were the
43 dominant sources of net surface PM_{2.5} in Beijing and Tianjin, constituting a total of 86.2%
44 and 92.9%, respectively, while emissions, horizontal transport, and aerosol processes
45 dominated the net surface PM_{2.5} in Shijiazhuang and Baoding. In addition, the EPs in
46 Beijing and Tianjin were primarily driven by local emissions, while the EPs in
47 Shijiazhuang and Baoding were attributed to combined local emissions and regional
48 transport. The reductions in PM_{2.5} in Case 2 relative to Case 1 were attributed to the weaker
49 PM_{2.5} formation from emissions and aerosol processes. However, the EPs were enhanced
50 by low planetary boundary layer heights, low vertical export of PM_{2.5} from the boundary
51 layer to the free troposphere, and substantial horizontal import, especially in Shijiazhuang
52 and Baoding. This study improves the understanding of buildup of PM_{2.5} during the EPs,
53 and the results provide insights for designing more effective emissions control strategies
54 to mitigate future PM_{2.5} episodes.

55 **Keywords:** Fine particulate matter; Pollution episodes; Process analysis; WRF-CMAQ;
56 COVID-19 shutdown.

57

58

59 **1. Introduction**

60 For more than two decades, China has been suffering from severe haze pollution,
61 attributed to its population growth, urbanization, fast industrialization, as well as economic
62 advancement (Li et al., 2020; Shi et al., 2017; Zhao et al., 2021). The development of severe
63 haze is caused by a combination of anthropogenic emissions (local and regional)
64 (Sulaymon et al., 2020, 2021a) and adverse meteorological conditions (Chen et al., 2021;
65 Hua et al., 2021; Hu et al., 2016; Shen, et al., 2021; Shi et al., 2020; Sulaymon et al., 2021a,
66 2021b). Severe air pollution causes reductions in visibility (Jiang et al., 2021; Li et al.,
67 2019; Wang et al., 2018), changes in climate and ecosystem services (Jiang et al., 2021;
68 Zhao et al., 2021), and adverse human health effects (Chen et al., 2017; Croft et al., 2019;
69 Hopke et al., 2019; Shang et al., 2018; Shen et al., 2020; Yan et al., 2018). The global
70 disease burden (GDB) has attributed about 2 million premature deaths per annum to severe
71 air pollution exposure in China (Yin et al., 2020).

72 The issuance of the new ambient air quality standards (GB3095-2012) in 2012 and
73 the subsequent implementation of the Air Pollution Prevention and Control Action Plan
74 (APPCAP) in September 2013 by the Chinese authorities has led to reduction in the
75 concentrations of fine particulate matter with aerodynamic diameters of ≤ 2.5 (PM_{2.5}) in
76 Chinese cities (Fan et al., 2020; Sulaymon et al., 2021d; Wang et al., 2016). For instance,
77 Xue et al. (2019) noted about 32.5% reduction in the national population-weighted PM_{2.5}
78 annual mean between 2013 and 2017. However, high PM_{2.5} concentrations are still
79 observed in most cities, with annual averages violating the annual Grade I (15 $\mu\text{g}/\text{m}^3$) and
80 Grade II (35 $\mu\text{g}/\text{m}^3$) Chinese Ambient Air Quality Standards (CAAQS), and much higher
81 than the WHO (5 $\mu\text{g}/\text{m}^3$) recommended limit or the USEPA (12 $\mu\text{g}/\text{m}^3$) standard.

82 The Beijing-Tianjin-Hebei (BTH) region that includes Beijing and Tianjin, and
83 Hebei Province, is one of the most economically developed regions in China. The region
84 has been suffering from severe PM_{2.5} pollution over the past two decades (Chang et al.,
85 2018; Dai et al., 2021a), particularly during the winter season. During past international
86 events (e.g. 2008 Olympic Games, 2014 Asia-Pacific Economic Cooperation, and the 2015
87 Military Parade), Chinese authorities implemented major emissions reductions measures
88 in the BTH region to improve air quality. The effectiveness and success of the emissions
89 reduction policies have been assessed (Wang et al., 2016; Xu et al., 2017; Yang et al., 2016).

90 In December 2019, an outbreak of coronavirus disease (COVID-19) occurred in
91 Wuhan (Zhu et al., 2020) and spread across China and many other countries within a short
92 time. As one of the measures to curtail the spread of COVID-19 pandemic in China, a
93 nationwide lockdown was implemented by the Chinese authorities, leading to significant
94 reductions in anthropogenic emissions and PM_{2.5} concentrations across China (Sulaymon
95 et al., 2021a, 2021c; Wang et al., 2020; Zhao et al., 2020; Zhao et al., 2021). However, the
96 BTH region still experienced high PM_{2.5} pollution episodes during the lockdown
97 (Sulaymon, et al., 2021a; Zhang et al., 2021). Compared to the past international events
98 held in Beijing during the summer and autumn seasons (with no or few pollution episodes),
99 the COVID-19 pandemic occurred in winter, a period with frequent severe pollution events
100 especially in the BTH region. In addition, the COVID-19 lockdown had a longer period
101 with very strict measures than the duration of the past three events.

102 Previous studies have assessed the impacts of COVID-19 lockdown on air quality
103 as well as the relationships between air quality and meteorological conditions during
104 lockdown in BTH region (Cui et al., 2020; Dai et al., 2020; 2021b; Sulaymon et al., 2021a;

105 Zhang et al., 2021; Zhao et al., 2021), other regions in China (Gao et al., 2021; Liu et al.,
106 2020; Shen et al., 2021a, 2021b; Sulaymon, et al., 2021c; Wang et al., 2020; Wu et al.,
107 2021; Xing et al., 2020), and outside mainland China (Bashir et al., 2020; Chauhan and
108 Singh, 2020, 2021; Mishra et al., 2021; Muhammad et al., 2020; Orak and Ozdemir, 2021;
109 Querol et al., 2021; Sharma et al., 2020; Singh and Chauhan, 2020; Srivastava, 2021; Ye
110 et al., 2022). A few studies have also been performed on the regional source apportionment
111 of PM_{2.5} during the lockdown (Li et al., 2020; Ma et al., 2021). Li et al. (2020) reported
112 that industry (32.2-61.1%) and residential (2.1-28.5%) were the two highest sources
113 contributing to PM_{2.5} in the Yangtze River Delta (YRD) region, while about 14.0-28.6%
114 contribution was due to long-range transport from northern China. In the BTH region, a
115 few studies have also investigated the source apportionment of PM_{2.5} during lockdown (Cui
116 et al., 2020; Dai et al., 2020). For example, Dai et al. (2020) used Positive Matrix
117 Factorization (PMF) to investigate the sources of PM_{2.5} in Tianjin. Their results showed
118 that secondary inorganic aerosols (SIA) (50.5%), fireworks and residential burning
119 (32.0%), and primary coal combustion emissions (13.3%) were the three dominant sources
120 contributing to PM_{2.5} during the lockdown. Overall, previous studies have reported
121 persistent haze episodes in the BTH region during lockdown despite the emission
122 reductions, and have generally attributed them to unfavorable meteorological conditions
123 (Cui et al., 2020; Dai et al., 2020; 2021b; Sulaymon et al., 2021a; Zhang et al., 2021; Zhao
124 et al., 2021). However, the formation of air pollutants involves various physical processes
125 (such as emissions, condensation, advection, diffusion, deposition, etc.) as well as
126 oxidative chemical process (Huang et al., 2005; Wang et al., 2014; Ye et al., 2022).

127 The process analysis (PA) tool in the Community Multiscale Air Quality (CMAQ)
128 chemical transport model can provide quantitative analysis of the individual contributions
129 of various physical and chemical processes to the observed air pollution (Liu et al., 2010;
130 Liu and Zhang, 2011; Xing et al., 2011; Ye et al., 2022). Liu and Zhang (2011) employed
131 the PA tool to analyze a regional PM_{2.5} pollution episode in the U.S. They found that
132 emissions and aerosol processes such as homogeneous nucleation, heterogeneous
133 nucleation, and condensation were the dominant contributors to increased PM_{2.5}
134 concentrations, while horizontal and vertical transport and dry deposition were the primary
135 loss mechanisms. Liu et al. (2010) utilized the PA to explore the contributions of various
136 atmospheric processes on ozone and PM₁₀ concentrations in China during four seasons.
137 The results showed that emissions and aerosol processes were the main contributors to
138 PM₁₀ concentrations, while horizontal transport was the major removal pathway. Xing et
139 al. (2011) used CMAQ-PA tool to quantify the air quality benefits from emissions
140 reductions and meteorological variations during the 2008 Beijing Olympics. The results
141 indicated that aerosol and emission processes acted as the major PM_{2.5} pathways, while
142 vertical transport was the major PM_{2.5} sink at the surface.

143 Therefore, analyzing the air quality during the unique lockdown period to provide
144 additional understanding of the underlying causes of high pollution episodes even during
145 periods of substantially reduced anthropogenic activity is important for providing
146 approaches to future air quality management strategies. The present study is the first that
147 elucidated the contributions of various atmospheric processes to PM_{2.5} pollution episodes
148 during the lockdown in the BTH region. The results provide new insights into PM_{2.5}
149 formation of the three pollution episodes during lockdown. Thus, it provides a valuable

150 example of how to use opportunities like the lockdown period to better understand the
151 causal factors of episodes in other areas of the world, which can then be applied to develop
152 more effective control strategies that would reduce the magnitude of these episodes and
153 better protect public health.

154 **2. Methodology**

155 *2.1. Model set-up and configurations*

156 The Community Multiscale Air Quality model version 5.2 (CMAQv5.2) was
157 applied to simulate the air quality in the BTH region during the COVID-19 lockdown
158 period (January 24-February 29, 2020). The photochemical mechanism and the aerosol
159 module used in configuring the model were the State-wide Air Pollution Research Center
160 version 07 (SAPRC07tic) and AERO6i, respectively (Liu et al., 2020; Sulaymon et al.,
161 2021a, 2021b). Two nested domains with horizontal resolutions of 36 and 12 km were used
162 (Fig. S1). The outer domain (36 km) covers China and the surrounding regions (137 x 107
163 grids), and the inner domain (12 km) covers the study area, the BTH region (127 x 202
164 grids). Each of the two domains had 18 vertical layers, emanating from the surface to a
165 height of about 20 km above the ground level. The initial and boundary conditions (IC/BC)
166 used in the 36 km domain were based on the default profiles provided by the CMAQ model,
167 while the IC/BC used for the 12 km domain were generated from the results of the 36 km
168 simulations. As a way of reducing the impact of initial conditions on PM_{2.5} predictions, the
169 simulations began on January 19, and the results of the first 5 days (January 19-23, 2020)
170 were excluded from the model analysis, thus serving as a spin-up of the model. The
171 meteorological inputs were simulated by the Weather Research and Forecasting (WRF v4.0)
172 model with the FNL reanalysis data serving as the IC/BC. The detailed settings and

173 configurations, including the major physics schemes used in this study are listed in Table
174 S1, while other settings could be found in previous studies where the WRF model was
175 applied (Hu et al., 2015, 2016; Wang et al., 2021).

176 In this study, the Multi-resolution Emission Inventory for China (MEIC) of year
177 2016 (<http://www.meicmodel.org>) served as the anthropogenic emissions from China. In
178 addition, the anthropogenic emissions from adjacent countries and regions were processed
179 based on the Regional Emission inventory in ASia version 2 (REAS2) (Kurokawa et al.,
180 2013). Biogenic emissions were estimated with the Model of Emissions of Gases and
181 Aerosols from Nature (MEGAN) version 2.1. Open burning emissions were generated
182 based on the data obtained from the Fire INventory from NCAR (FINN) (Wiedinmyer et
183 al., 2011). Sea salt and windblown emissions were generated inline (Sulaymon et al., 2021a,
184 2021b). Further details regarding the emission processing can be found in Hu et al. (2016)
185 and Qiao et al. (2015).

186 To evaluate the impacts of the emissions reductions on air quality, two scenarios
187 (referred to as Cases 1 and 2) were simulated as presented in Table S2. The first scenario
188 (Case 1) used the original MEIC16 emission inventory. In the second scenario (Case 2),
189 emissions from transportation, industry, and power sectors were reduced (Table S2) during
190 the lockdown period, while those of residential and agriculture were similar to Case 1. The
191 basis for adopting the emission reduction factors has been previously presented (Sulaymon
192 et al., 2021a; Wang et al., 2020), and has also been detailed in the Supplementary Material
193 (Text S1). The differences between the results of Cases 1 and 2 represent the impact of
194 emissions reductions on air quality during the lockdown.

195

196 2.2. *Process analysis*

197 The process analysis (PA) tool embedded in the CMAQ model has been described
198 as a versatile analytical tool for quantifying the contributions of individual atmospheric
199 processes and chemical reactions to a pollutant (Fu et al., 2020; Ye et al., 2022). PA is
200 comprised of two components; the integrated process rate (IPR) and integrated reaction
201 rate (IRR) analysis. The IPR involves the changes in the hourly concentrations of pollutants
202 due to individual atmospheric processes such as gas-phase chemistry, emissions, aerosol
203 processes, dry deposition, cloud processes, and vertical and horizontal transport at each
204 grid cell in the model domain. The IPR analysis has been extensively used in quantifying
205 the contributions individual atmospheric processes to air pollutants (Fan et al., 2015; Fu et
206 al., 2020; Li et al., 2012; Wang et al., 2010; Xing et al., 2011; Ye et al., 2022), hence,
207 detailed information about IPR can be found in these referenced studies.

208 In this study, the IPR module in CMAQv5.2 was employed to resolve both physical
209 and chemical processes involved in the formation of PM_{2.5} during the lockdown period in
210 the BTH region. The IPR results were subsequently used to analyze the individual
211 processes involved in PM_{2.5} formation in the surface layer and full planetary boundary
212 layer (PBL), respectively. For this purpose, the processes considered were the chemistry
213 (gas-phase), emissions, aerosol processes (SOA formation, nucleation, condensation,
214 coagulation, heterogeneous chemistry, mode merging, and aerosol thermodynamics), cloud
215 processes, dry deposition, vertical transport (sum of vertical advection and diffusion), and
216 horizontal transport (sum of horizontal advection and diffusion). Based on their
217 contributions to PM_{2.5} concentrations, atmospheric processes can be grouped into two;
218 source process (concentration increases) and sink process (concentration decreases). Dry

219 deposition and emission belong to the sink and source process, respectively. The IPR of
220 other processes can either be source (positive) or sink (negative). The contributions of
221 individual atmospheric processes to the formation of PM_{2.5} were estimated using the
222 approach of Ye et al. (2022):

$$223 \quad \text{SOURCE}_p = \frac{\sum_t \text{IPR}_{p,t}}{\sum_p \sum_t \text{IPR}_{p,t}} \times 100\% \quad (\text{IPR}_{p,t} > 0) \quad (1)$$

$$224 \quad \text{SINK}_p = \frac{\sum_t \text{IPR}_{p,t}}{\sum_p \sum_t \text{IPR}_{p,t}} \times 100\% \quad (\text{IPR}_{p,t} < 0) \quad (2)$$

225 where p is the atmospheric process, and t is the time (in hour). SOURCE_p and SINK_p are
226 the proportions of the atmospheric process p in all source and sink processes, respectively.
227 Both source and sink categories are used to reveal how important an atmospheric process
228 is in influencing the changes in PM_{2.5} concentrations.

229 **3. Results and discussion**

230 *3.1. WRF model performance*

231 Meteorological parameters play an important role in the formation and
232 transportation of air pollution (Hu et al., 2016; Sulaymon et al., 2021a, 2021b; Wang et al.,
233 2021). In addition, the influences of meteorological parameters on the air quality
234 simulations using chemical transport model have also been established (Hu et al., 2016;
235 Sulaymon et al., 2021a; Wang et al., 2021). To evaluate the WRF model performance, the
236 predicted temperature (T2) and relative humidity (RH) at 2 m above ground level, and wind
237 speeds (WS) and wind directions (WD) at 10 m above surface were compared to the
238 observational data downloaded from the official website of the Chinese Meteorological
239 Agency (<http://data.cma.cn/en>, last access: January 2023). Table S3 shows the summary

240 statistics including the mean observation (OBS), mean prediction (PRE), mean bias (MB),
241 mean error (ME), and the root mean square error (RMSE). In addition to the BTH region
242 as a whole, four representative cities including Beijing (BJ), Tianjin (TJ), Shijiazhuang
243 (SJZ), and Baoding (BD) were evaluated. Generally, T2 (Table S3) was slightly over-
244 predicted in the BTH and the four representative cities during the lockdown. The MB and
245 ME of T2 in BTH were 0.4 and 1.7, respectively, which fell below the suggested
246 benchmarks ($MB \leq \pm 0.5$; and $ME \leq 2.0$) (Emery et al., 2001). These are consistent with a
247 previous study over BTH region (Chang et al., 2019). Except in Tianjin (MB:0.5), the MB
248 values in other three cities (Beijing:2.2; Shijiazhuang:0.6; and Baoding:1.3) exceeded the
249 benchmark. Except in Beijing (ME:2.3), the ME values in all the cities were within the
250 benchmark range. Although there were no suggested benchmarks for the MB and ME
251 indices of RH, however, RH (Table S3) was underpredicted in BTH region and the four
252 representative cities (Ma et al., 2021). Similar results had been reported by previous studies
253 over BTH region (Chang et al., 2018; Li et al., 2021b; Sulaymon et al., 2021a; Zhao et al.,
254 2021) and China as a whole (Hu et al., 2016; Sulaymon et al., 2021b; Wang et al., 2021).
255 Bhati and Mohan (2018) obtained a similar result and attributed it to the influence of the
256 boundary layer parameterization on the weather prediction. The mean observed WS across
257 the cities and BTH ranged from 1.8 to 2.3 m/s, an illustration of relatively calm conditions
258 during the lockdown. Generally, WS (Table S3) was over-predicted (Ma et al., 2021).
259 However, based on the ME, MB, and RMSE indices, the predictions reasonably captured
260 the observations across the four cities and BTH (Li et al., 2021b; Sulaymon et al., 2021a;
261 Zhao et al., 2021). The over-predictions of WS might be due to unresolved topography
262 within the WRF model (Li et al., 2014). The MB values met the suggested benchmark

263 ($\leq \pm 0.5$) in BTH and three cities except Shijiazhuang (0.7). During the lockdown, the ME
264 and RMSE values ranged between 0.6-0.9 and 0.7-1.2, respectively, with both indices
265 falling below the recommended benchmarks (≤ 2.0). WD (Table S3) was generally under-
266 predicted except in Shijiazhuang where the PRE was slightly higher than the OBS. Overall,
267 the MB values were above the suggested criterion range ($\leq \pm 10$) except in Baoding (MB: -
268 0.8), Shijiazhuang (MB:2.3), and BTH (MB: -9.6). Also, the ME values in the four cities
269 and BTH region greatly exceeded the benchmark ($\leq \pm 30$), especially in Shijiazhuang
270 (ME:101.5), Beijing (ME:78.4), and BTH region (ME:70.5). Similar model performance
271 of WD had been reported (Hu et al., 2016; Sulaymon et al., 2021a, 2021b; Wang et al.,
272 2021). Generally, in this study, the WRF model exhibited better performance when
273 compared to previous studies in BTH region (Chang et al., 2019; Li et al., 2021b; Sulaymon
274 et al., 2021a; Zhang et al., 2021; Zhao et al., 2021) and China as a country (Ma et al., 2021;
275 Sulaymon et al., 2021b; Wang et al., 2021). Since the simulated meteorological parameters
276 were robust, they were used in driving the air quality simulations.

277

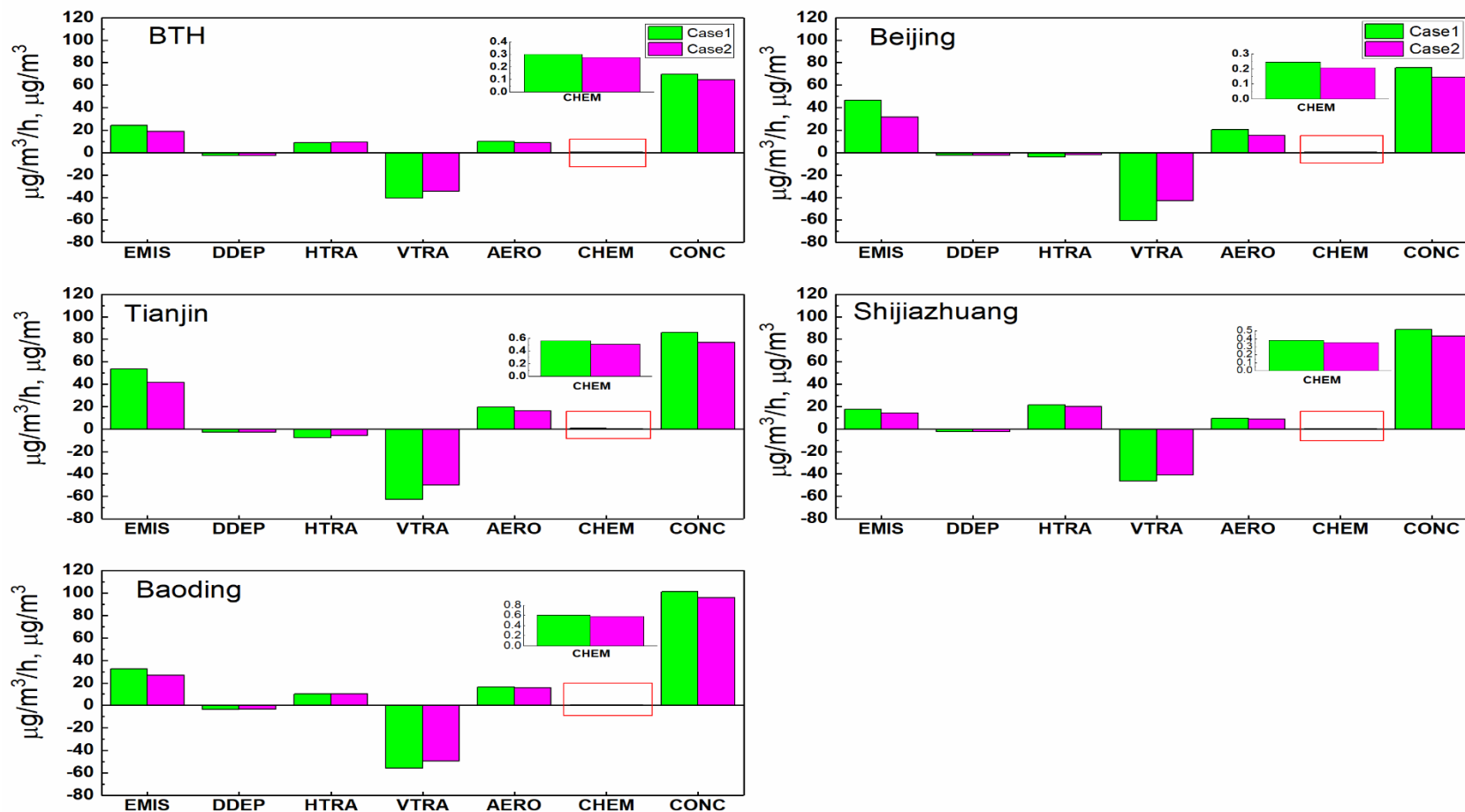
278 3.2. *CMAQ model performance*

279 In evaluating the performance of CMAQ model in predicting $PM_{2.5}$, statistical
280 indices, which include the mean observations (OBS), mean predictions (PRE), mean
281 fractional bias (MFB), mean fractional error (MFE), mean normalized bias (MNB), and
282 mean normalized error (MNE) were calculated. The performance of CMAQ model for
283 $PM_{2.5}$ over the BTH and at four representative cities during the lockdown period based on
284 the two cases are shown in Table S4. Generally, the simulated $PM_{2.5}$ concentrations
285 exhibited good agreement with the observed data with the model performance indices

286 falling within the recommended benchmarks for $PM_{2.5}$ ($MFB \leq \pm 0.60$ and $MFE \leq 0.75$)
287 (Boylan and Russel, 2006) in BTH and the four cities for the two cases. For Case 1, $PM_{2.5}$
288 was over-estimated in BTH (0.10), Beijing (0.31), and Tianjin (0.41), while it was under-
289 predicted in Shijiazhuang (-0.05) and Baoding (-0.19). Considering Case 2, all of the MFB
290 values were negative except in Tianjin (0.32), an indication that CMAQ under-predicted
291 the total $PM_{2.5}$ concentrations in BTH and the other three cities. Chang et al. (2019) had
292 reported an under-estimation of $PM_{2.5}$ by CMAQ in Beijing and Shijiazhuang, which is
293 consistent with this study for Case 2. Also, the model performances for Case 2 are in line
294 with the findings of Sulaymon et al. (2021a) In addition, under-predictions of $PM_{2.5}$ in all
295 of the prefectural-level cities of BTH region were reported by Jiang et al. (2021). The MFE
296 values for the two cases ranged between 0.40-0.51, which were within the recommended
297 benchmark ($MFE \leq 0.75$). Overall, the CMAQ model has shown better performance in this
298 study when compared to previous studies across the BTH region (Chang et al., 2019; Jiang
299 et al., 2021; Li et al., 2021b; Sulaymon et al., 2021a; Zhang et al., 2021; Zhao et al., 2021).
300 Thus, the model results were deemed acceptable for further analyses, including the IPR
301 analysis.

302 3.3. *IPR analysis of $PM_{2.5}$ formation at the surface layer*

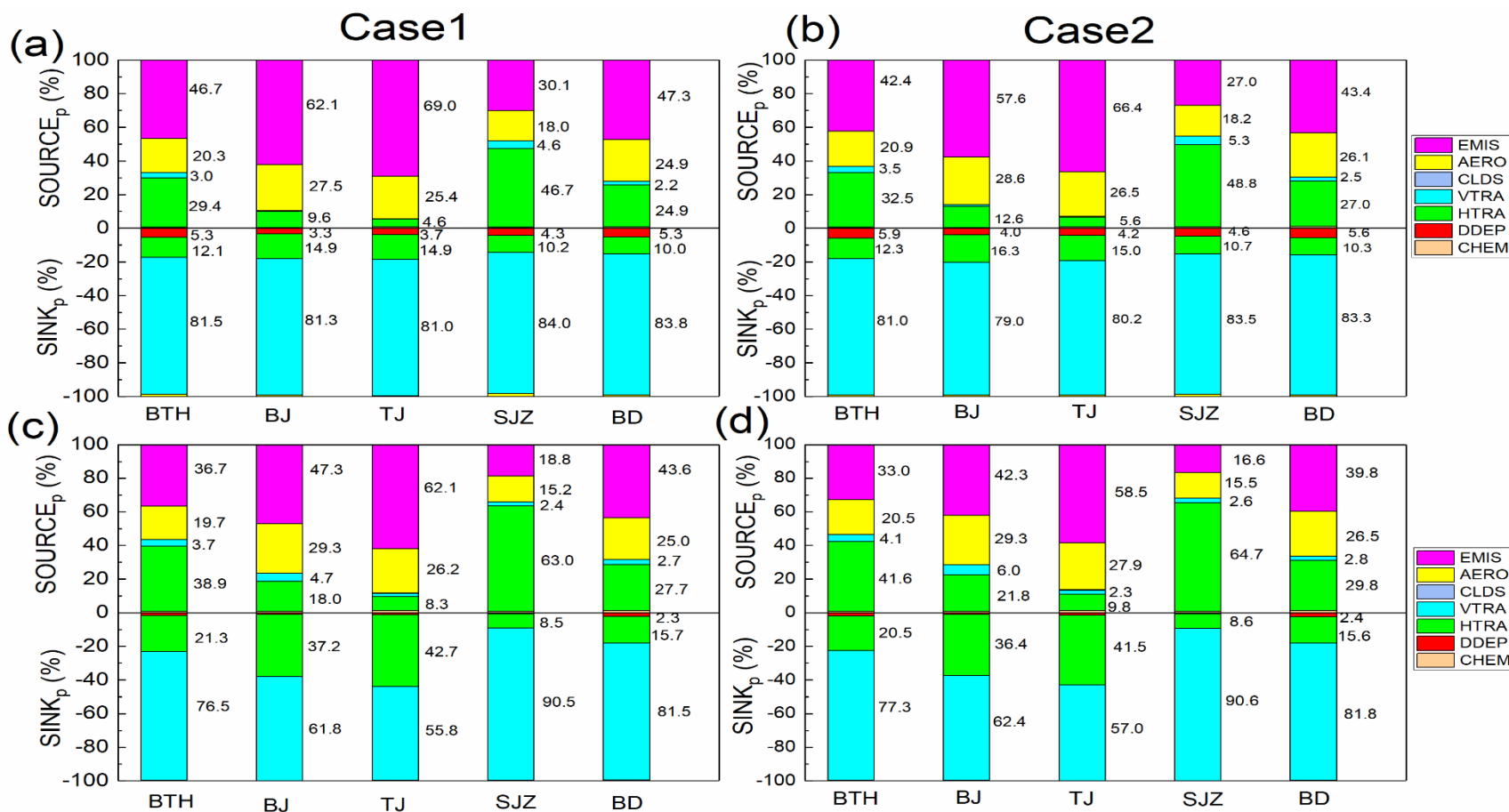
303 The hourly concentrations of $PM_{2.5}$ as well as the contributions of the individual
304 atmospheric processes to the evolution of $PM_{2.5}$ at the surface layer in the BTH region and
305 four representative cities for the two cases during the lockdown period are illustrated in
306 Fig. 1. In the BTH region as a whole, the emissions (EMIS), horizontal transport (HTRA),
307 and aerosol processes (AERO) were the major positive contributors (sources) to the net
308 surface $PM_{2.5}$.



309
 310 **Fig. 1.** Contributions of the individual processes to the concentrations of PM_{2.5} at the surface layer in Cases 1 and 2 during the lockdown
 311 period. EMIS represents PM_{2.5} input by emissions, DDEP represents PM_{2.5} decrease by dry deposition; HTRA and VTRA represent
 312 PM_{2.5} change by horizontal and vertical transport, respectively; AERO represents PM_{2.5} change by the aerosol; and CHEM represents
 313 PM_{2.5} change by gas-phase chemistry. The unit of the processes is $\mu\text{g}/\text{m}^3/\text{h}$. CONC is the hourly PM_{2.5} concentrations in $\mu\text{g}/\text{m}^3$.

314 For Case 2, the contributions of EMIS, HTRA, and AERO to $PM_{2.5}$ formation were 42.4,
315 32.5, and 20.9% (Fig. 2b), respectively, while their contributions in the same order for Case
316 1 were 46.7, 29.4, and 20.3% (Fig. 2a), respectively. The reduction in the surface layer's
317 $PM_{2.5}$ for the two cases was primarily attributed to the vertical transport (VTRA), while
318 slight removal was also due to dry deposition (DDEP). In Beijing and Tianjin, EMIS and
319 AERO were the predominant processes that contributed to the net surface $PM_{2.5}$ formation
320 (Fig. 1) for both cases. The total contribution ratios of EMIS and AERO in Case 2 were
321 86.2% and 92.9% for Beijing and Tianjin (Fig. 2b), respectively. The reduction of surface
322 $PM_{2.5}$ in Beijing and Tianjin for the two cases was associated with the VTRA, HTRA, and
323 DDEP processes, with VTRA being the highest sink, with negative contributions of 79.0-
324 81.3% (Beijing) and 80.2-81.0% (Tianjin). The results of the present study are consistent
325 with those reported by Ye et al. (2022) in the coastal city of Kannur, India, where the EMIS,
326 HTRA, and AERO were the dominant processes that positively contributed to $PM_{2.5}$
327 evolution, while VTRA and DDEP were responsible for surface $PM_{2.5}$ removal during the
328 three periods considered in the study. Also, Fan et al. (2015) reported EMIS and VTRA as
329 the two major processes that influenced $PM_{2.5}$ at the surface layer in the Pearl River Delta
330 (PRD) region of China. Furthermore, Liu et al. (2010) and Xing et al. (2011) had earlier
331 reported EMIS and AERO as the major $PM_{2.5}$ sources in both surface layer and the PBL in
332 Beijing, while Xing et al. (2011) found VTRA as the major $PM_{2.5}$ sink in the surface layer.
333 The $PM_{2.5}$ removal due to HTRA and DDEP in both cases were relatively the same in both
334 Beijing and Tianjin. Considering Shijiazhuang and Baoding, similar trends were obtained
335 regarding the contributions of individual processes to $PM_{2.5}$ formation.

336
337



338
 339 **Fig. 2.** Positive and negative contribution ratios of the individual processes to $PM_{2.5}$ concentrations (a,b) at the surface layer and (c,d)
 340 in the planetary boundary layer in Cases 1 and 2 during the lockdown period. EMIS, AERO, CLDS, VTRA, HTRA, DDEP, and CHEM
 341 represent the contributions of the emissions, aerosol, clouds, vertical transport, horizontal transport, dry deposition, and gas-phase
 342 chemistry, respectively to $PM_{2.5}$ formation.

343 The EMIS, AERO, and HTRA processes dominated the positive contributions to
344 the net surface $PM_{2.5}$ in the two cities (Fig. 1), accounting for a total of 94.0 and 96.5% in
345 Shijiazhuang and Baoding, respectively in Case 2 (Fig. 2b), while similar contributions
346 were obtained in Case 1 (Fig. 2a). In addition to EMIS and AERO processes, the horizontal
347 import of $PM_{2.5}$ to the surface layer via HTRA contributed to the elevated $PM_{2.5}$
348 concentrations in both Shijiazhuang and Baoding relative to Beijing and Tianjin. VTRA
349 dominated the removal of $PM_{2.5}$ from the surface layer to upper layers in both cities, with
350 higher rates in Case 1 relative to Case 2. DDEP process also had negative effects on $PM_{2.5}$
351 formation in the two cities, with very low contributions, especially in Shijiazhuang. The
352 photochemistry (CHEM) process had positive net impacts on $PM_{2.5}$ evolution for the two
353 cases across the BTH region and the four representative cities, however, the contributions
354 were extremely low and negligible (Fan et al., 2015). This is contrary to what was reported
355 in Kannur (Ye et al., 2022), as CHEM had negative effects on $PM_{2.5}$ in the city. Due to the
356 negligible contributions of cloud (CLDS) processes to $PM_{2.5}$, it was not discussed in this
357 study. It should be noted that the $PM_{2.5}$ concentrations in BTH region and the four cities in
358 Case 2 were relatively low compared to Case 1. This could be attributed to low $PM_{2.5}$
359 formation from EMIS in Case 2. However, there was no substantive decrease in $PM_{2.5}$
360 concentrations in Case 2 despite reductions in anthropogenic emissions. This could be
361 explained by the reduced $PM_{2.5}$ export from the surface layer to the upper layers due to low
362 VTRA rates in Case 2 (compared to Case 1), leading to the accumulation of $PM_{2.5}$ in the
363 surface layer, which subsequently led to high $PM_{2.5}$ pollution during the lockdown period.

364

365

366 3.4. *IPR analysis of PM_{2.5} formation in the PBL*

367 Fig. S2 shows the mean hourly change rates attributed to individual atmospheric
368 processes to PM_{2.5} production and the concentrations of PM_{2.5} in the PBL during the
369 lockdown. The contributions of the various processes to PM_{2.5} formation within the PBL
370 in BTH and the four cities followed the similar trends as found in the surface layer.
371 However, the contributions of the individual processes to PM_{2.5} were smaller in the PBL
372 compared to the surface layer, as PM_{2.5} concentrations decrease as vertical layers increase
373 (Fan et al., 2015). Generally, the contributions of EMIS and VTRA to the net PM_{2.5} (Case
374 2) were low in the PBL compared to the surface layer. For instance, relative to what was
375 obtained to the surface layer, the rates due to EMIS and VTRA in the PBL decreased by
376 half in BTH region and all of the representative cities. Similar to the surface layer, the
377 EMIS, HTRA, and AERO were the predominant contributors to the net PM_{2.5} in the whole
378 BTH region and Baoding, while only EMIS and AERO processes contributed substantially
379 to the net PM_{2.5} in Beijing and Tianjin. In Shijiazhuang, however, HTRA was the dominant
380 contributor to PM_{2.5} formation. Compared to other processes, the contributions of CHEM
381 process were extremely low and negligible (Fan et al., 2015; Ye et al., 2022). In addition
382 to VTRA as the major process responsible for the removal of PM_{2.5} across the study areas,
383 PM_{2.5} removal in Beijing and Tianjin was also associated with HTRA. In all of the study
384 areas, slight removal of PM_{2.5} was also attributed to DDEP process. It could be noted that
385 the VTRA and HTRA effects within the PBL were opposite to those to the surface layer.
386 As illustrated in Fig. 2(d), the negative contributions (sinks) due to VTRA in the entire
387 PBL substantially reduced in all of the study areas except Shijiazhuang (increased) when
388 compared to the surface layer. Contrary to the surface layer, the sinks (PM_{2.5} removal) due

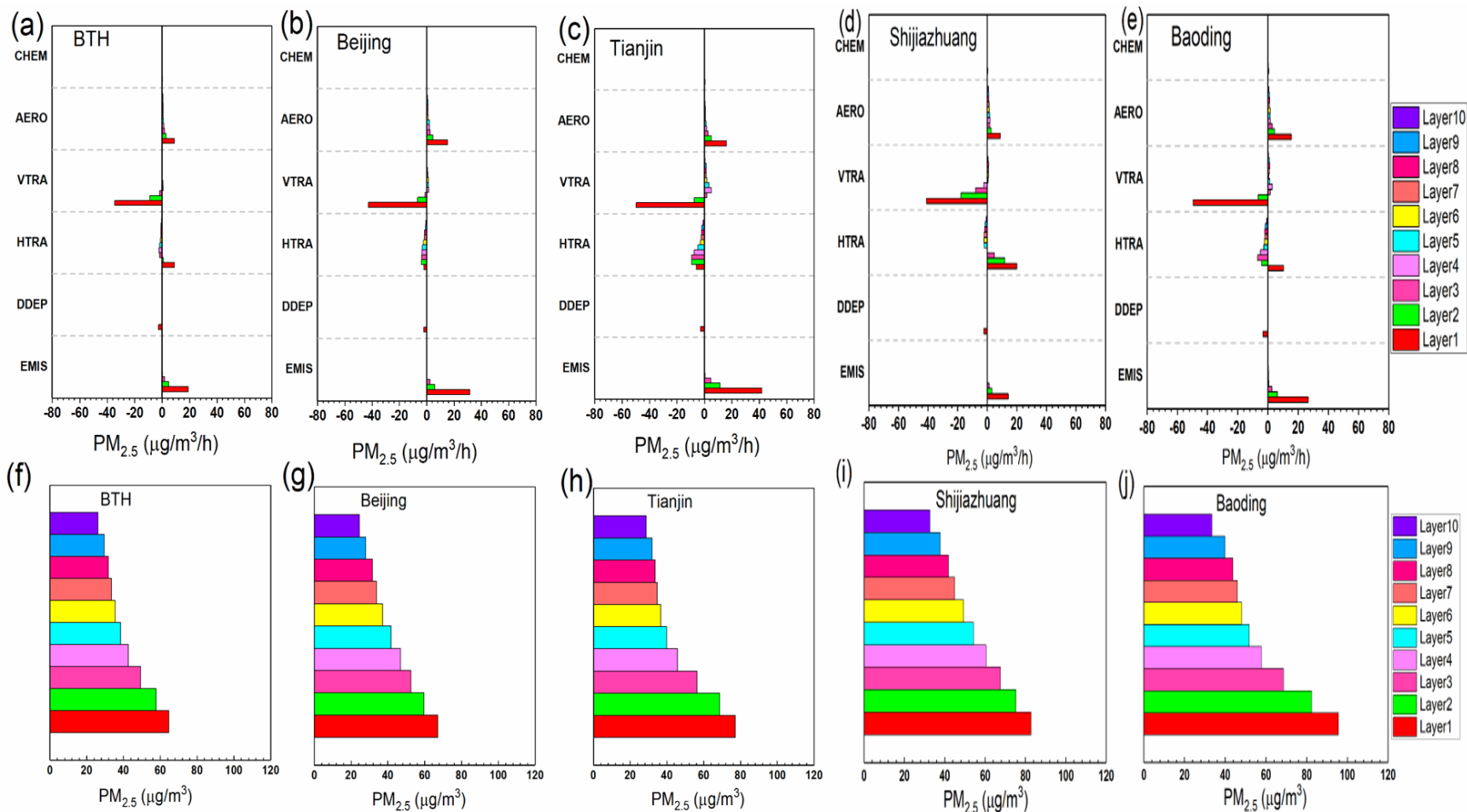
389 to HTRA within the PBL increased in all of the study areas except Shijiazhuang
390 (decreased). It is worth noting that despite the decreases in EMIS rates by half (which might
391 have adversely influenced PM_{2.5} formation within the PBL) in comparison to the surface
392 layer, the absolute difference in PM_{2.5} concentrations between the surface layer and PBL
393 was not significant, and ranged between 5.7-9.1 µg/m³ across the study areas. This could
394 be attributed to reduced PM_{2.5} export due to low VTRA rates, leading to the accumulation
395 of PM_{2.5} within the PBL, and subsequently resulted to high PM_{2.5} concentrations. Overall,
396 in the PBL, EMIS and VTRA served as the two dominant processes that impacted PM_{2.5}
397 in BTH, Beijing, Tianjin, and Baoding, while VTRA and HTRA were the two major
398 processes that influenced PM_{2.5} formation in Shijiazhuang.

399 3.5. *Vertical profiles of the atmospheric processes contributing to PM_{2.5}*

400 The mean hourly PM_{2.5} change rates attributed to individual atmospheric processes
401 for the first ten layers (layers 1-10), as well as the vertical profiles of PM_{2.5} evolution for
402 Case 2 during the lockdown period are illustrated in Fig. 3, while that of Case 1 are shown
403 in Fig. S3. As earlier stated in section 3.4, the characteristics of PM_{2.5} concentrations at
404 upper layers (layer 4 and above) were different from near-surface layers, hence, the
405 contributions of emissions sources at upper layers were negligible (Fan et al., 2015). Across
406 the study areas, the contributions from EMIS sources were only found within layers 1-3
407 (Fig. 3a-e) (Fan et al., 2015; Ye et al., 2022), and this was associated with the height of the
408 emissions sources (Fan et al., 2015; Ye et al., 2022). The highest and lowest contributions
409 of EMIS were found in Tianjin and Shijiazhuang, respectively, and the contribution
410 decreased as the vertical layer increased. Within the first three layers, AERO process was
411 another major source of PM_{2.5} in all of the study areas, and the formation rate of PM_{2.5}

412 through the AERO process decreased as the vertical layer increased. Furthermore, VTRA
413 contributed negatively and served as the predominant sink for removing the near-surface
414 $PM_{2.5}$ at the lower layers in Beijing (layers 1-3), Shijiazhuang (layers 1-4), Tianjin and
415 Baoding (layers 1-2), while it slightly contributed positively (acted as source) at the upper
416 layers. This is consistent with the results of Fan et al. (2015), in which VTRA was reported
417 as a sink in the near-surface layers and a source in the upper layers (layer 4 and above). In
418 Beijing (Fig. 3b) and Tianjin (Fig. 3c), HTRA served as another sink for $PM_{2.5}$ across the
419 vertical layers, and the rate initially increased between layers 1 and 2, but continuously
420 decreased as the vertical layer increased. In Shijiazhuang (Fig. 3d), HTRA contributed
421 positively at the lower layers (layers 1-3) and negatively at the upper layers. Considering
422 Baoding (Fig. 3e), HTRA only acted as the source at the first layer, while it behaved as the
423 sink from the second layer upward. It could be deduced that there were vertical and
424 horizontal exports of $PM_{2.5}$ in Beijing and Tianjin at the surface layer, while Shijiazhuang,
425 Baoding, and the whole BTH region witnessed vertical export and horizontal import of
426 $PM_{2.5}$ in the surface layer. DDEP acted as another sink of $PM_{2.5}$, and only existed at the
427 first layer across the study areas (Fan et al., 2015; Ye et al., 2022). DDEP contributions
428 were only found in the first layer because dry deposition was treated as a bivariate variable
429 by the CMAQ model, and integrated it over the whole atmospheric column (Fan et al.,
430 2015). As shown in Fig. 3(f-j), the highest $PM_{2.5}$ concentration was found in the surface
431 layer, and decreased with increases in vertical layer height (Fan et al., 2015). This result
432 could be attributed to the contributions of EMIS and AERO processes, as well as the
433 decreasing trends of the two processes as the vertical layer increased.

434



435

436 **Fig. 3.** Hourly PM_{2.5} change rates due to individual atmospheric processes for layers 1-10 (a-e) and evolution of hourly PM_{2.5} vertical
 437 profiles (f-j) in Case 2 during the lockdown period. Abbreviations used in this figure are the same as in Fig. 1.

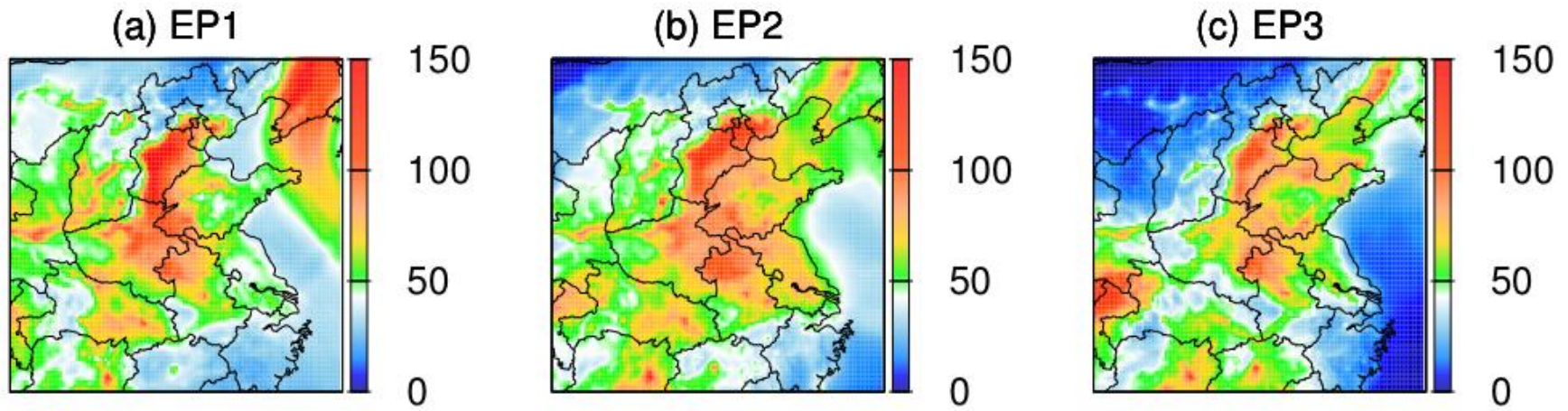
438

439 3.6 *IPR analysis of PM_{2.5} pollution episodes during lockdown*

440 During the lockdown period, the predicted PM_{2.5} concentrations (in Case 2) (Fig.4;
441 Tables S5-S6) indicated that persistent PM_{2.5} pollution episodes could not be avoided in
442 the BTH region despite reductions in anthropogenic emissions (Sulaymon et al., 2021a).
443 Fig. S6 illustrates the spatial distributions of PM_{2.5} in the BTH region during the lockdown
444 for the two cases. Fig. S6(b) shows that the PM_{2.5} concentrations during the lockdown were
445 higher (PM_{2.5} ≥ 75 µg/m³, level II of Chinese air quality standard) in Tianjin and southern
446 Hebei Province, while the northern Hebei was characterized with low concentrations
447 (PM_{2.5} ≤ 50 µg/m³). In the prefectural-level cities of BTH region, three severe PM_{2.5}
448 pollution episodes (EPs) (Fig. 4) occurred during the lockdown (Case 2). They are
449 represented as EP1 (January 24-31, 2020), EP2 (February 7-13), and EP3 (February 19-
450 21). It should be noted that EP1 and EP2 coincided with the 2020 Spring (January 25) and
451 Lantern (February 8) festivals, respectively. The statistics for all the EPs in each city are
452 enumerated in Tables S5-S6. For the purpose of process analysis of PM_{2.5} during the EPs,
453 Beijing, Tianjin, Shijiazhuang, and Baoding were selected as the representative cities. As
454 illustrated in Fig. 5, Beijing and Tianjin had the highest PM_{2.5} concentrations during EP2,
455 while Shijiazhuang and Baoding recorded their highest PM_{2.5} concentrations during EP1.
456 Also, during EP2 and EP3, Baoding experienced severe pollution with elevated PM_{2.5}
457 concentrations. This indicates that the region suffered severe pollution episodes during the
458 lockdown. Dai et al. (2021) and Sulaymon et al. (2021a) had previously reported severe
459 haze episodes in the BTH region during the lockdown. Therefore, it becomes pertinent to
460 elucidate the major atmospheric processes responsible for the formation of the EPs.

461

462



463

464 **Fig. 4.** Spatial distributions of predicted PM_{2.5} (Case 2) during (a) EP1, (b) EP2, and (c) EP3 in the BTH region. Units are µg/m³.

465

466

467

468

469

470

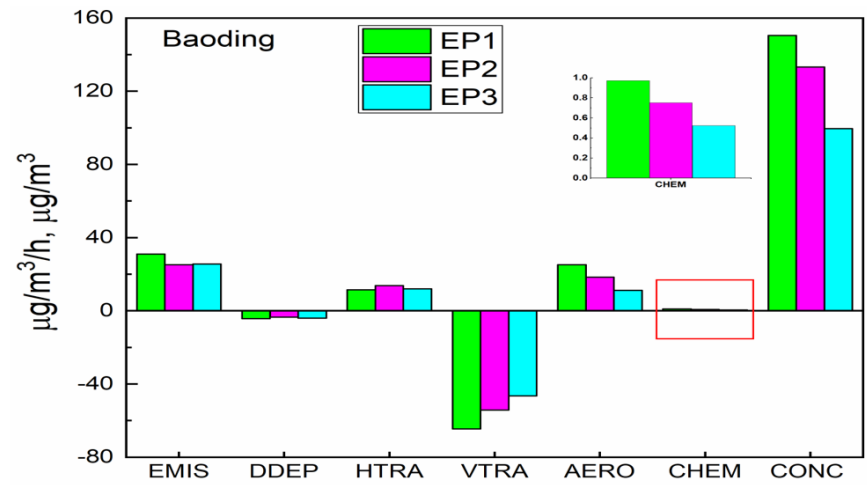
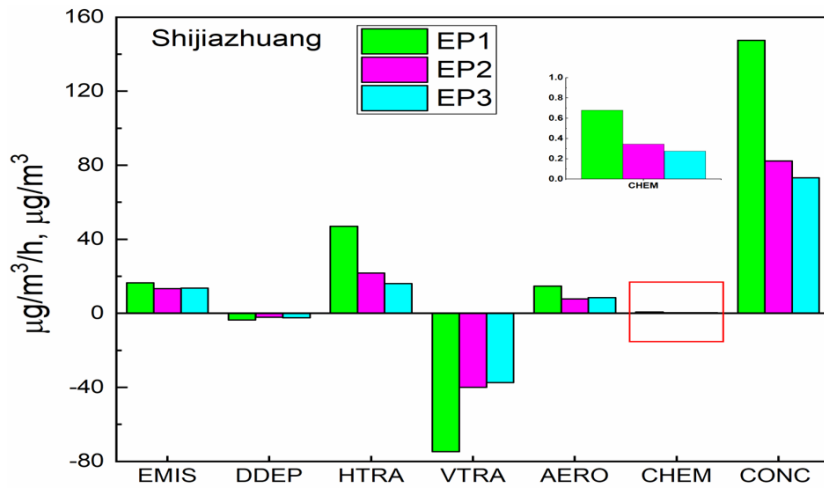
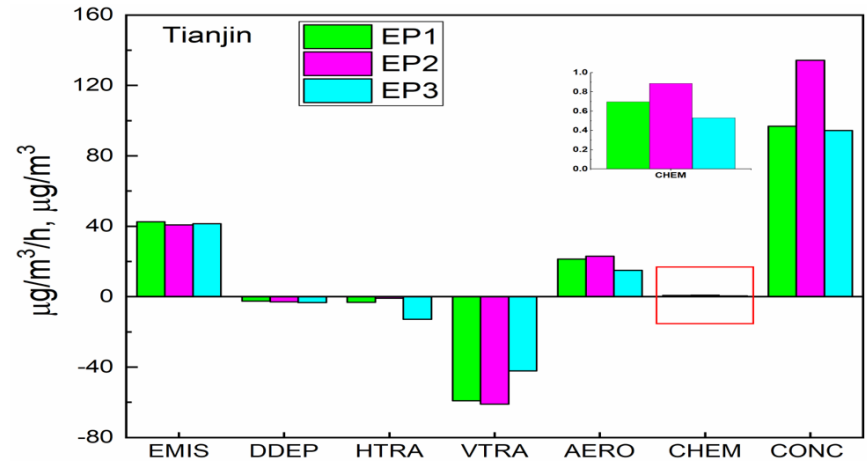
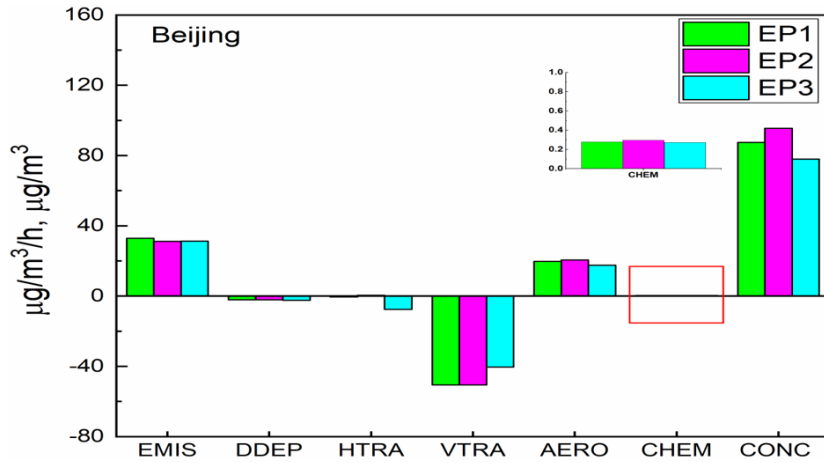
471

472

473

474

475



476

477 **Fig. 5.** Contributions of the individual processes to the concentrations of $\text{PM}_{2.5}$ (Case 2) at the surface layer during the three pollution
 478 episodes in the four representative cities. Abbreviations used in this figure are the same as in Fig. 1.

479 The contributions of different atmospheric processes to PM_{2.5} formation (in Case 2) during
480 the three EPs in the four representative cities were analyzed. Table S7 shows the average
481 planetary boundary layer height (PBLH) and wind speed for the four cities during the three
482 EPs. The PBLH during the third pollution episode (EP3; PBLH>400 m) was higher than
483 the PBLH during the first two pollution episodes (EP1 and EP2; PBLH<370 m) across the
484 study areas. A thinner boundary layer is more conducive for the accumulation of locally-
485 emitted particles, leading to increased PM_{2.5} concentrations and results in haze events (Fan
486 et al., 2015). As illustrated in Fig. 5, the three pollution episodes in Beijing and Tianjin
487 were principally caused by local emissions (EMIS), while the pollution events in
488 Shijiazhuang and Baoding could be attributed to both local emissions (EMIS) and regional
489 transport (HTRA).

490 Fig. 5 shows that emissions sources and aerosols were the major positive
491 contributors to PM_{2.5} pollution in Beijing, Tianjin, and Baoding, while horizontal transport
492 was the most significant positive contributor to pollution level in Shijiazhuang, followed
493 by emissions and aerosols. In Baoding, however, HTRA also contributed positively
494 towards PM_{2.5} concentrations throughout the three episodes. There were no significant
495 differences between emissions sources among the three episodes in all of the study areas,
496 and the average total emissions ranged between 13.3-42.6 µg/m³/h across the EPs in the
497 cities. During the three episodes across the four cities, PM_{2.5} was released into the
498 atmosphere through EMIS and AERO processes, and fell back to the surface layer via
499 DDEP process (Fan et al., 2015), with very low rates of dry deposition (ranged between -
500 2.1 µg/m³/h and -4.3 µg/m³/h). Also, PM_{2.5} was transported and diffused through VTRA
501 and HTRA processes. In Beijing and Tianjin, there were negligible differences between

502 the contributions from VTRA during the first two episodes, and the total rates were
503 approximately $-51 \mu\text{g}/\text{m}^3/\text{h}$ and $-60 \mu\text{g}/\text{m}^3/\text{h}$ in Beijing and Tianjin, respectively. During
504 EP3 in the two cities, the contributions by VTRA ($-40 \mu\text{g}/\text{m}^3/\text{h}$ in Beijing; and $-42 \mu\text{g}/\text{m}^3/\text{h}$
505 in Tianjin) were low relative to the first two episodes. The VTRA contributions in
506 Shijiazhuang ($-75 \mu\text{g}/\text{m}^3/\text{h}$) and Baoding ($-65 \mu\text{g}/\text{m}^3/\text{h}$) during EP1 were greater than those
507 contributed in Beijing and Tianjin during the same period, and this was due to lower PBLH
508 values (Table S7) in Shijiazhuang and Baoding relative to Beijing and Tianjin. The
509 difference in the VTRA rates between the first two episodes and the third episode in Beijing
510 and Tianjin could be explained by the accumulation of particulates on near-surface layers
511 due to the nature of boundary layer (thinner) (Fan et al., 2015) being exhibited during the
512 first two pollution episodes. Therefore, VTRA had a greater clearing impact for $\text{PM}_{2.5}$
513 during the first two episodes in the two cities. Contrarily, during the third episode in the
514 two cities, a more uniform vertical mixing of $\text{PM}_{2.5}$ was achieved, and this was due to the
515 thicker PBLHs during EP3 (Table S7). Hence, the clearing effect of VTRA during EP3
516 was low compared to EP1 and EP2. In addition, due to higher wind speed during EP3
517 (Table S7), the negative contributions due to HTRA were higher in Beijing ($-8 \mu\text{g}/\text{m}^3/\text{h}$)
518 and Tianjin ($-13 \mu\text{g}/\text{m}^3/\text{h}$) during EP3 compared to EP1 and EP2, and this subsequently
519 reduced the contributions from VTRA during EP3. In Shijiazhuang, VTRA also exhibited
520 a very greater clearing effect during EP1 than EP2 and EP3, and similar scenario also
521 occurred in Baoding. In Shijiazhuang, HTRA was the dominant positive contributor to
522 $\text{PM}_{2.5}$ throughout the episodes, with the highest contribution rate during EP1. In Baoding,
523 however, there was negligible difference between the contributions from HTRA to $\text{PM}_{2.5}$
524 pollution during the three episodes. Due to availability of several emissions sources in

525 Beijing and Tianjin, which result to a large quantity of local emissions, $PM_{2.5}$
526 concentrations were generally higher in the two cities. Hence, the effects of both VTRA
527 and HTRA on pollution levels were negative during the three pollution episodes, and both
528 mainly provided dilution and clearing effects in the two cities (Fan et al., 2015). On the
529 other hand, in both Shijiazhuang and Baoding, horizontal transport contributed positively
530 and significantly increased $PM_{2.5}$ concentrations during the three episodes. It is also worthy
531 to mention that $PM_{2.5}$ concentrations during the three episodes in the four cities were
532 greatly and positively influenced by the planetary boundary layer height, as the episode
533 with the lowest PBLH had the highest $PM_{2.5}$ concentration in a city. The results of the
534 present study are consistent with those reported by Fan et al. (2015) during three pollution
535 episodes over the PRD region. Fan et al. (2015) had reported surface emissions, aerosol
536 processes, and horizontal transport as the major contributors to air pollution episodes over
537 the PRD. In the PBL (Fig. S7), EMIS and AERO were also the dominant contributors to
538 $PM_{2.5}$ concentrations in Beijing and Tianjin, HTRA was the most important source in
539 Shijiazhuang, and EMIS, AERO, and HTRA actively contributed to $PM_{2.5}$ formation in
540 Baoding during the EPs. VTRA was the major removal pathway. However, the
541 contribution and removal rates were low in the PBL relative to the surface layer.

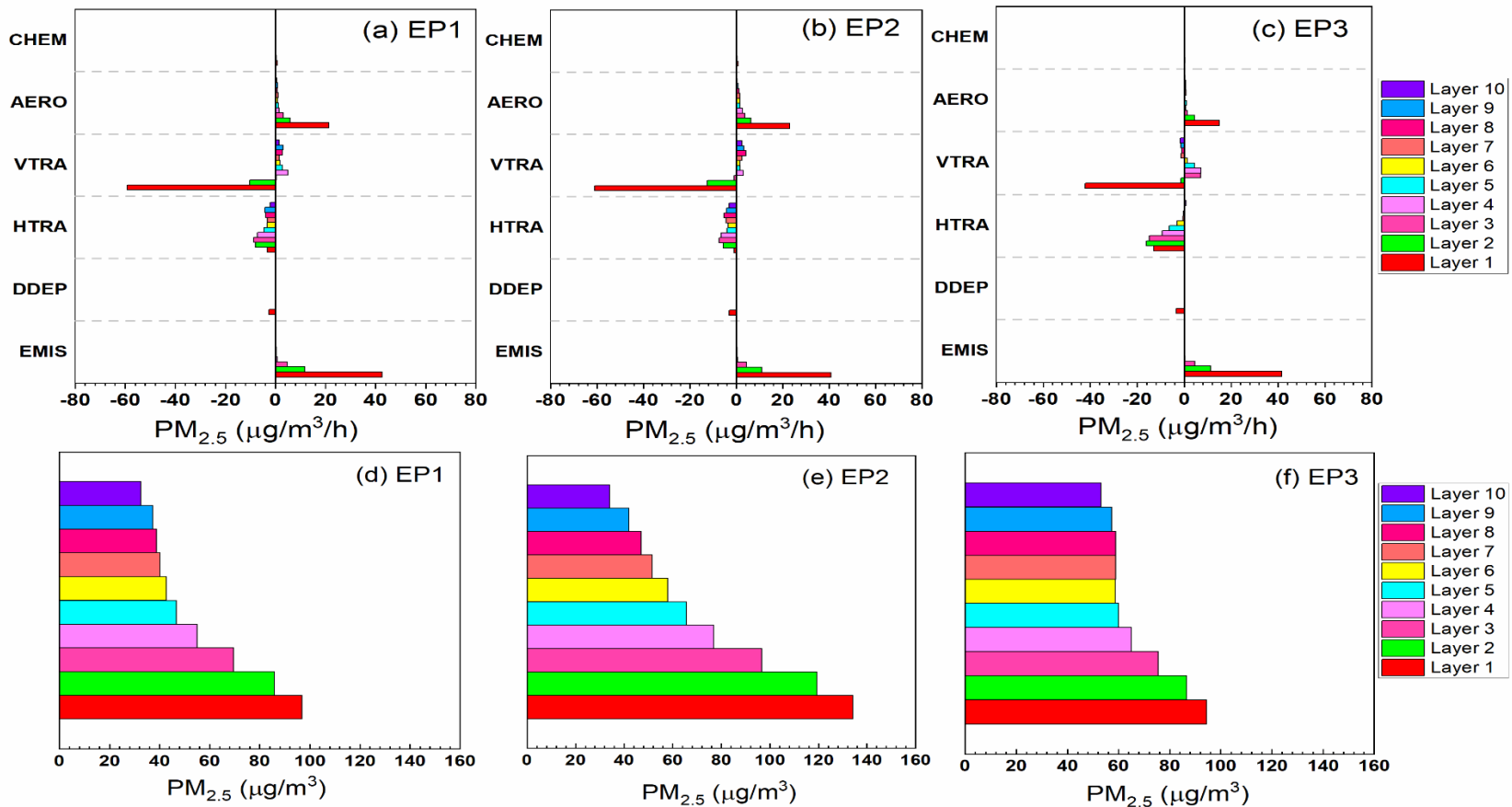
542 To better understand the roles of the atmospheric processes towards the pollution
543 episodes, $PM_{2.5}$ formation and removal within the PBL (layers 1-10) were analyzed in
544 Tianjin (Fig. 6), while those of other three cities are illustrated in Figs S8-S10. Considering
545 the three EPs in Tianjin, the positive contributions of EMIS and AERO processes to the
546 hourly $PM_{2.5}$ significantly occurred within layers 1-3 (Fig. 6a-c), while they both
547 contributed less at upper layers. Also, there were vertical imports of $PM_{2.5}$ (although very

548 low) at upper layers (layers 3-10 for EP1 and EP2; and layers 3-6 for EP3). Conversely,
549 VTRA (layers 1-2) and HTRA (layers 1-10) served as the predominant sinks and $PM_{2.5}$
550 removal pathways. DDEP process also acted as another sink for $PM_{2.5}$ during the EPs, and
551 only existed at the first layer (Fan et al., 2015). The contributions by CHEM process were
552 negligible across the vertical layers (Fan et al., 2015; Ye et al., 2022). As shown in Fig.
553 6(d-f), EP2 was characterized with the highest $PM_{2.5}$ concentrations, followed by EP1 and
554 EP3. Furthermore, the $PM_{2.5}$ formation processes in the surface layer during the EPs were
555 compared. Fig. 7 illustrates the percentage contributions of the atmospheric processes to
556 $PM_{2.5}$ formation/removal during the EPs in the four cities. The total contributions of EMIS
557 and AERO (EMIS+AERO) during the EPs ranged between 80-89% and 88-97% in Beijing
558 (Fig. 7a) and Tianjin (Fig. 7b), respectively. In Shijiazhuang (Fig. 7c), the contributions
559 due to HTRA during the episodes ranged between 44-61%, making it the major $PM_{2.5}$
560 source. As earlier revealed in Fig. 5, $PM_{2.5}$ formation during the episodes in Baoding (Fig.
561 7d) was attributed to the contributions of EMIS, AERO, and HTRA, with total
562 contributions of 93-98% during the EPs. In the four cities, $PM_{2.5}$ removal was dominantly
563 influenced by VTRA during the EPs.

564 Furthermore, the diel variations of the contributions of various atmospheric
565 processes to the formation of $PM_{2.5}$ as well as the hourly variations of $PM_{2.5}$ concentrations
566 at the surface layer during the three episodes are illustrated in Fig. 8. In Beijing, EMIS and
567 AERO processes were the major $PM_{2.5}$ sources, and showed two peaks (07:00 LT and
568 20:00 LT) during the three episodes.

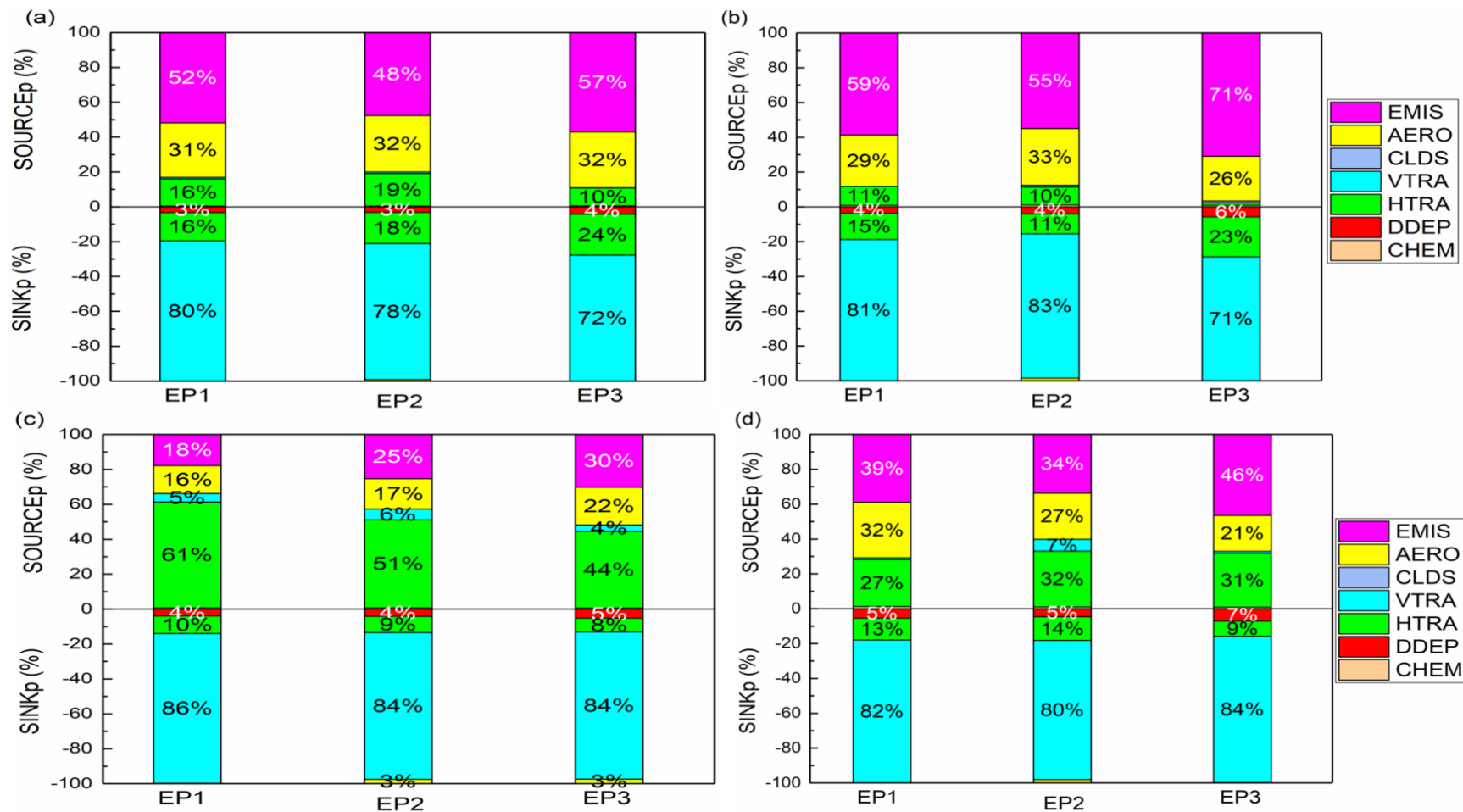
569

570



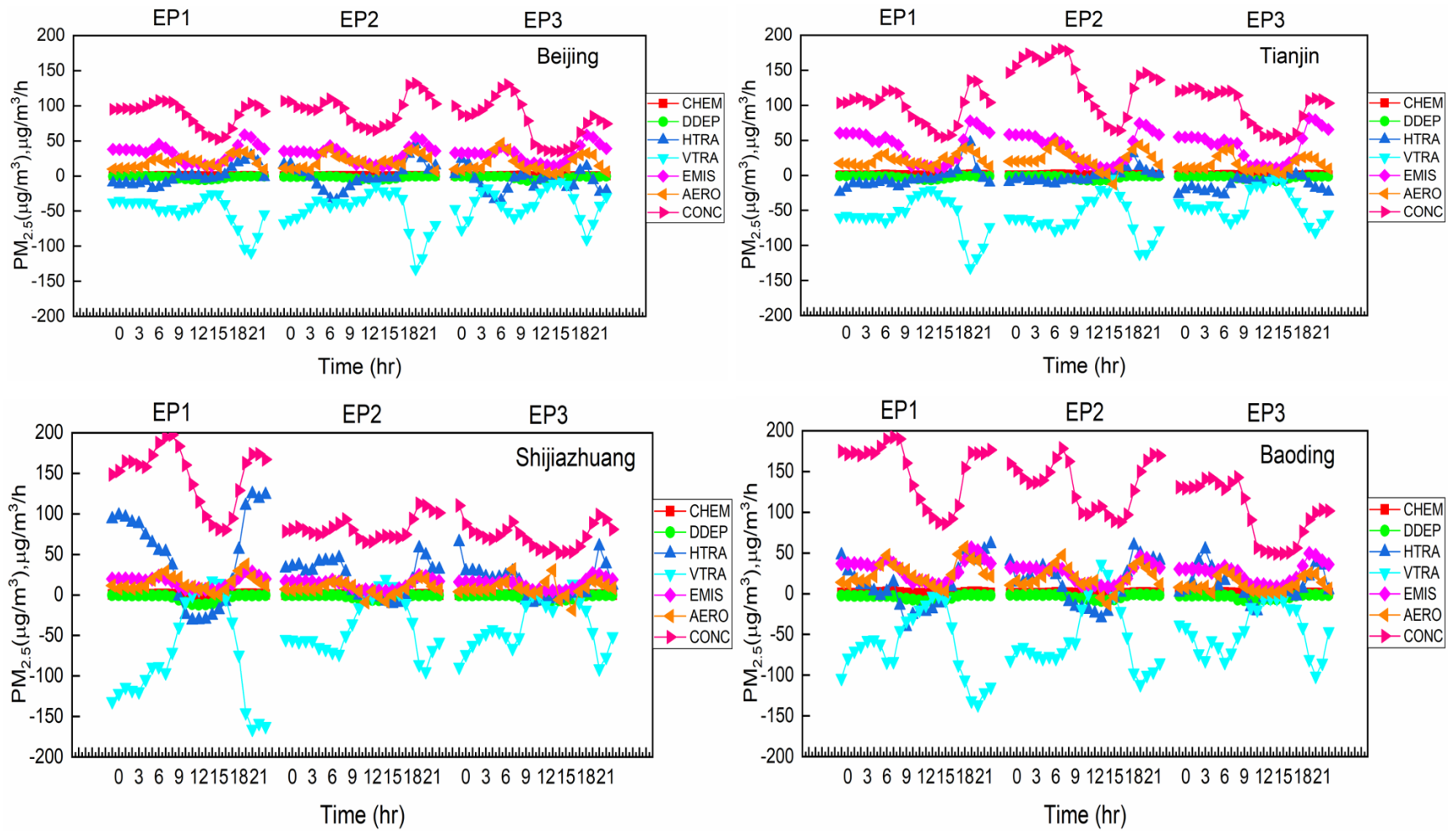
571

572 **Fig. 6.** Hourly PM_{2.5} change rates (Case 2) due to individual atmospheric processes for layers 1-10 (a-c) and evolution of hourly PM_{2.5}
 573 vertical profiles (d-f) during the three pollution episodes in Tianjin. Abbreviations used in this figure are the same as in Fig. 1.
 574



575
 576 **Fig. 7.** Positive and negative contribution ratios of the individual processes to PM_{2.5} concentrations (Case 2) at the surface layer in (a)
 577 Beijing, (b) Tianjin, (c) Shijiazhuang, and (d) Baoding during the three pollution episodes. Abbreviations used in this figure are the
 578 same as in Fig. 2.

579



580

581 **Fig. 8.** Diel variations of contributions of individual processes to PM_{2.5} formation (Case 2) at the surface layer during the three pollution
 582 episodes in the four representative cities. Abbreviations used in this figure are the same as in Fig. 1.

583 The highest rates of EMIS during the EPs ranged between 54.8-58.6 $\mu\text{g}/\text{m}^3/\text{h}$, all occurred
584 at 20:00 LT. The VTRA dominated the $\text{PM}_{2.5}$ removal, with the highest removal rates of -
585 109.3 $\mu\text{g}/\text{m}^3/\text{h}$ (at 21:00 LT), -132.6 $\mu\text{g}/\text{m}^3/\text{h}$ (at 20:00 LT), and -90.7 $\mu\text{g}/\text{m}^3/\text{h}$ (at 20:00
586 LT) during EP1, EP2, and EP3, respectively. In addition, HTRA was another major $\text{PM}_{2.5}$
587 removal pathway during the EPs. However, HTRA later acted as another $\text{PM}_{2.5}$ source
588 during EP1 (17:00-22:00 LT; with maximum rate of 29.6 $\mu\text{g}/\text{m}^3/\text{h}$ at 21:00 LT), EP2
589 (00:00-03:00 and 18:00-23:00 LT; with maximum rate of 44.7 $\mu\text{g}/\text{m}^3/\text{h}$ at 20:00 LT), and
590 EP3 (00:00-02:00 and 19:00-20:00 LT; with highest rate of 24.0 $\mu\text{g}/\text{m}^3/\text{h}$ at 01:00 LT),
591 leading to the horizontal import of $\text{PM}_{2.5}$ during the periods. Considering Tianjin, EMIS
592 process was the dominant $\text{PM}_{2.5}$ source and exhibited two distinct peaks (00:00 LT and
593 20:00 LT) during the three episodes. The highest contributions of EMIS during EP1, EP2,
594 and EP3 were 77.7 $\mu\text{g}/\text{m}^3/\text{h}$, 74.1 $\mu\text{g}/\text{m}^3/\text{h}$, and 81.7 $\mu\text{g}/\text{m}^3/\text{h}$, respectively, all occurred at
595 20:00 LT. AERO process was another $\text{PM}_{2.5}$ source with two peaks during EP1 (07:00 LT
596 and 19:00 LT), EP2 and EP3 (07:00 LT and 20:00 LT). The negative contributions of
597 VTRA made it the dominant $\text{PM}_{2.5}$ sink throughout the 24hrs period, with the maximum
598 removal rates of -132.1 $\mu\text{g}/\text{m}^3/\text{h}$ (at 20:00 LT), -112.5 $\mu\text{g}/\text{m}^3/\text{h}$ (at 20:00 LT), and -81.3
599 $\mu\text{g}/\text{m}^3/\text{h}$ (at 21:00 LT) during EP1, EP2, and EP3, respectively. Besides VTRA, HTRA
600 served as the second major $\text{PM}_{2.5}$ sink during the three EPs. However, HTRA later became
601 another $\text{PM}_{2.5}$ source during EP1 (16:00-21:00 LT; with maximum rate of 47.5 $\mu\text{g}/\text{m}^3/\text{h}$),
602 EP2 (14:00-23:00; with maximum rate of 31.1 $\mu\text{g}/\text{m}^3/\text{h}$), and EP3 (17:00-18:00 LT; with
603 very low rates). In Shijiazhuang, HTRA was the major $\text{PM}_{2.5}$ contributor, and showed two
604 peaks during EP1 (98.3 $\mu\text{g}/\text{m}^3/\text{h}$ at 01:00 LT and 124.8 $\mu\text{g}/\text{m}^3/\text{h}$ at 21:00 LT), EP2 (45.8
605 $\mu\text{g}/\text{m}^3/\text{h}$ at 08:00 LT and 57.8 $\mu\text{g}/\text{m}^3/\text{h}$ at 20:00 LT), and EP3 (65.2 $\mu\text{g}/\text{m}^3/\text{h}$ at 00:00 LT

606 and $60.3 \mu\text{g}/\text{m}^3/\text{h}$ at 21:00 LT). The VTRA was the dominant $\text{PM}_{2.5}$ removal pathway, with
607 the highest rates of $-165.6 \mu\text{g}/\text{m}^3/\text{h}$, $-94.5 \mu\text{g}/\text{m}^3/\text{h}$, and $-91.0 \mu\text{g}/\text{m}^3/\text{h}$ during EP1, EP2, and
608 EP3, respectively, all at 21:00 LT. However, VTRA later became positive and served as
609 another $\text{PM}_{2.5}$ source during EP1 (13:00-16:00 LT; with maximum rate of $17.4 \mu\text{g}/\text{m}^3/\text{h}$ at
610 15:00 LT), EP2 (14:00-17:00 with maximum rate of $19.4 \mu\text{g}/\text{m}^3/\text{h}$ at 15:00 LT), and EP3
611 (15:00-17:00 with highest rate of $13.6 \mu\text{g}/\text{m}^3/\text{h}$ at 17:00 LT), resulting to the vertical import
612 of $\text{PM}_{2.5}$ during the periods. In Baoding, EMIS, AERO, and HTRA were the major $\text{PM}_{2.5}$
613 formation pathways during nighttime, while EMIS and AERO were the dominant sources
614 during daytime. Being the major $\text{PM}_{2.5}$ removal pathway, VTRA had the highest rates of -
615 $136.3 \mu\text{g}/\text{m}^3/\text{h}$ (21:00 LT), $-111.4 \mu\text{g}/\text{m}^3/\text{h}$ (20:00 LT), and $-101.1 \mu\text{g}/\text{m}^3/\text{h}$ (21:00 LT)
616 during EP1, EP2, and EP3, respectively. During EP2, VTRA shortly behaved as another
617 $\text{PM}_{2.5}$ source (13:00-15:00 LT, with highest rate of $36.5 \mu\text{g}/\text{m}^3/\text{h}$. With very low rates
618 during the episodes, DDEP and CHEM processes served as $\text{PM}_{2.5}$ sink and source,
619 respectively across the four cities. The $\text{PM}_{2.5}$ concentrations peaked in Beijing (EP1: 107.8
620 $\mu\text{g}/\text{m}^3$ at 07:00 LT; EP2: $132.1 \mu\text{g}/\text{m}^3$ at 20:00 LT; EP3: $130.3 \mu\text{g}/\text{m}^3$ at 08:00 LT), Tianjin
621 (EP1: $135.7 \mu\text{g}/\text{m}^3$ at 20:00 LT; EP2: $180.1 \mu\text{g}/\text{m}^3$ at 08:00 LT; EP3: $124.6 \mu\text{g}/\text{m}^3$ at 02:00
622 LT), Shijiazhuang (EP1: $197.6 \mu\text{g}/\text{m}^3$ at 09:00 LT; EP2: $112.6 \mu\text{g}/\text{m}^3$ at 20:00 LT; EP3:
623 $110.3 \mu\text{g}/\text{m}^3$ at 00:00 LT), and Baoding (EP1: $192.0 \mu\text{g}/\text{m}^3$ at 08:00 LT; EP2: $178.2 \mu\text{g}/\text{m}^3$
624 at 08:00 LT; EP3: $142.8 \mu\text{g}/\text{m}^3$ at 09:00 LT).

625 **4. Conclusions**

626 This study employed the PA tool in the CMAQ model to identify and quantify the
627 contributions of individual atmospheric processes and meteorology to the three $\text{PM}_{2.5}$
628 pollution episodes that occurred during the COVID-19 lockdown in the BTH region even

629 with the required reductions in human activities. Due to emission reductions, the total $PM_{2.5}$
630 concentrations across the BTH decreased by 6.2-11.0%. However, the region still
631 experienced three $PM_{2.5}$ pollution episodes during the lockdown. The IPR results showed
632 that the EMIS and AERO processes were the dominant positive contributors to the net
633 surface $PM_{2.5}$ in Beijing and Tianjin, while the EMIS, HTRA, and AERO pathways
634 dominated the net surface $PM_{2.5}$ formation in Shijiazhuang and Baoding. In Case 2, the
635 decrease in surface $PM_{2.5}$ concentrations across the BTH was primarily attributed to the
636 reduced EMIS and AERO processes, which shows the reduction in the primary source of
637 $PM_{2.5}$ as well as decrease in the formation of secondary aerosol through gas-to-particle
638 conversion. Both vertical and horizontal transport had significant impacts on the changes
639 in surface $PM_{2.5}$. Elevated $PM_{2.5}$ concentrations (in Case 2) in the BTH region during the
640 lockdown could be attributed to a low vertical transport rate of $PM_{2.5}$ from the surface layer
641 to the upper layers. Furthermore, during the three pollution episodes, EMIS and AERO
642 processes were the dominant sources of $PM_{2.5}$ formation in Beijing, Tianjin, and Baoding,
643 while HTRA was the major source in Shijiazhuang. In all of the four cities, vertical
644 transport served as the major $PM_{2.5}$ sink throughout the episodes, with differences in
645 vertical rates between the episodes in each city. The pollution levels in the four cities were
646 greatly and positively influenced by the PBLH, as the episode with the lowest PBLH had
647 the highest $PM_{2.5}$ concentration in a city. This study reveals the various atmospheric
648 processes and meteorological factors governing the $PM_{2.5}$ formation during the severe
649 pollution episodes in the BTH region, as well as the changes in the individual atmospheric
650 processes and $PM_{2.5}$ concentrations due to the lockdown measures, and shows that the
651 existing emissions control strategies could not prevent pollution episodes in the region,

652 especially during the winter period. Since it is not possible to control the aerosol and
653 transport processes, only further changes in emissions will reduce the severity of the
654 episodes. Thus, better forecasting of the conditions that would foment such episodes
655 combined with more effective emissions control strategies are urgently required to be able
656 to mitigate such future severe pollution episodes in the BTH region.

657

658 **Acknowledgements**

659 This work was supported by the National Natural Science Foundation of China (42007187).

660

661 **Conflict of Interest**

662 The authors declare that they have no conflict of interest.

663

664 **Open Research**

665 The simulated and the observation data (PM_{2.5} and meteorological variables) used in this
666 study for model evaluation and postprocessing (Figures and Tables) can be found in
667 Sulaymon et al. (2023).

668

669 **References**

- 670 Ambient air pollution (2021). Retrieved 28 October 2021, from
671 <https://www.who.int/airpollution/ambient/health-impacts/en>
672 Bashir, M. F., MA, B. J., Bilal, Komal, B., Bashir, M. A., Farooq, T. H., Iqbal, N., & Bashir,
673 M. (2020). Correlation between environmental pollution indicators and COVID-19
674 pandemic: A brief study in Californian context. *Environmental Research*, 187.
675 <https://doi.org/10.1016/j.envres.2020.109652>
676 Bhati, S., & Mohan, M. (2018). WRF-urban canopy model evaluation for the assessment
677 of heat island and thermal comfort over an urban airshed in India under
678 varying land use/land cover conditions. *Geoscience Letters*, 5(1).
679 <https://doi.org/10.1186/s40562-018-0126-7>

- 680 Boylan, J. W., & Russel, A. G. (2006). PM and light extinction model performance metrics,
681 goals, and criteria for three-dimensional air quality models. *Atmospheric*
682 *Environment*, 40, 4946-4959. <https://doi.org/10.1016/j.atmosenv.2005.09.087>
- 683 Chang, X., Wang, S., Zhao, B., Cai, S., & Hao, J. (2018). Assessment of inter-city transport
684 of particulate matter in the Beijing-Tianjin-Hebei region. *Atmospheric Chemistry*
685 *and Physics*, 18(7), 4843-4858. <https://doi.org/10.5194/acp-18-4843-2018>
- 686 Chang, X., Wang, S., Zhao, B., Xing, J., Liu, X., Wei, L., Song, Y., Wu, W., Cai, S., Zheng,
687 H., Ding, D., & Zheng, M. (2019). Contributions of inter-city and regional transport
688 to PM_{2.5} concentrations in the Beijing-Tianjin-Hebei region and its implications on
689 regional joint air pollution control. *Science of the Total Environment*, 660, 1191-
690 1200. <https://doi.org/10.1016/j.scitotenv.2018.12.474>
- 691 Chauhan A., & Singh, R.P. (2020). Decline in PM_{2.5} concentrations over major cities
692 around the world associated with COVID-19. *Environ. Res.* 187, 109634.
693 [10.1016/j.envres.2020.109634](https://doi.org/10.1016/j.envres.2020.109634)
- 694 Chauhan, A.K., & Singh, R.P. (2021). Effect of lockdown on HCHO and trace gases over
695 India during March 2020. *AAQR*, Volume 21, Issue 4, Article Number 200445.
696 [10.4209/aaqr.2020.07.0445](https://doi.org/10.4209/aaqr.2020.07.0445).
- 697 Chen, D., Xia, L., Guo, X., Lang, J., Zhou, Y., Wei, L., & Fu, X. (2021). Impact of inter-
698 annual meteorological variation from 2001 to 2015 on the contribution of regional
699 transport to PM_{2.5} in Beijing, China. *Atmospheric Environment*, 260.
700 <https://doi.org/10.1016/j.atmosenv.2021.118545>
- 701 Chen, L., Shi, M., Gao, S., Li, S., Mao, J., Zhang, H., Sun, Y., Bai, Z., & Wang, Z. (2017).
702 Assessment of population exposure to PM_{2.5} for mortality in China and its public
703 health benefit based on BenMAP. *Environmental Pollution*, 221, 311-317.
704 <https://doi.org/10.1016/j.envpol.2016.11.080>
- 705 Croft, D. P., Zhang, W., Lin, S., Thurston, S. W., Hopke, P. K., Masiol, M., Squizzato, S.,
706 van Wijngaarden, E., Utell, M. J., & Rich, D. Q. (2019). The association between
707 respiratory infection and air pollution in the setting of air quality policy and
708 economic change. *Annals of the American Thoracic Society*, 16(3), 321-330.
709 <https://doi.org/10.1513/AnnalsATS.201810-691OC>
- 710 Cui, Y., Ji, D., Maenhaut, W., Gao, W., Zhang, R., & Wang, Y. (2020). Levels and sources
711 of hourly PM_{2.5}-related elements during the control period of the COVID-19
712 pandemic at a rural site between Beijing and Tianjin. *Science of the Total*
713 *Environment*, 744. <https://doi.org/10.1016/j.scitotenv.2020.140840>
- 714 Dai, Q., Ding, J., Hou, L., Li, L., Cai, Z., Liu, B., Song, C., Bi, X., Wu, J., Zhang, Y., Feng,
715 Y., & Hopke, P. K. (2021). Haze episodes before and during the COVID-19
716 shutdown in Tianjin, China: Contribution of fireworks and residential burning.
717 *Environmental Pollution*, 286.
718 <https://doi.org/10.1016/j.envpol.2021.117252>
- 719 Dai, Q., Ding, J., Song, C., Liu, B., Bi, X., Wu, J., Zhang, Y., Feng, Y., & Hopke, P. K.
720 (2021). Changes in source contributions to particle number concentrations after
721 the COVID-19 outbreak: Insights from a dispersion normalized PMF.
722 *Science of the Total Environment*, 759.
723 <https://doi.org/10.1016/j.scitotenv.2020.143548>
- 724 Dai, Q., Liu, B., Bi, X., Wu, J., Liang, D., Zhang, Y., Feng, Y., & Hopke, P. K. (2020).
725 Dispersion normalized PMF provides insights into the significant changes in source

726 contributions to PM_{2.5} after the Covid-19 outbreak. *Environmental Science and*
727 *Technology*, 54(16), 9917-9927. <https://doi.org/10.1021/acs.est.0c02776>

728 Emery, C., Tai, E., & Yarwood, G. (2001). Enhanced Meteorological Modeling and
729 Performance Evaluation for Two Texas Ozone Episodes, Prepared for the Texas
730 Natural Resource Conservation Commission. Environ International Corporation,
731 Novato, CA.

732 Fan, Q., Lan, J., Liu, Y., Wang, X., Chan, P., Hong, Y., Feng, Y., Liu, Y., Zeng, Y.,
733 & Liang, G. (2015). Process analysis of regional aerosol pollution during spring in
734 the Pearl River Delta region, China. *Atmos. Environ.* 122, 829-838.

735 Fan, H., Zhao, C., & Yang, Y. (2020). A comprehensive analysis of the spatio-temporal
736 variation of urban air pollution in China during 2014-2018. *Atmospheric*
737 *Environment*, 220. <https://doi.org/10.1016/j.atmosenv.2019.117066>

738 Fu, X., Wang, T., Gao, J., Wang, P., Liu, Y., Wang, S., Zhao, B., & Xue, L. (2020). Persistent
739 heavy winter nitrate pollution by increased photochemical oxidants in Northern
740 China. *Environ. Sci. Technol.*, 54, 3881-3889.

741 Gao, C., Li, S., Liu, M., Zhang, F., Achal, V., Tu, Y., Zhang, S., & Cai, C. (2021). Impact
742 of the COVID-19 pandemic on air pollution in Chinese megacities from the
743 perspective of traffic volume and meteorological factors. *Science of the Total*
744 *Environment*, 773. <https://doi.org/10.1016/j.scitotenv.2021.145545>

745 Hopke, P. K., Croft, D., Zhang, W., Lin, S., Masiol, M., Squizzato, S., Thurston, S. W.,
746 van Wijngaarden, E., Utell, M. J., & Rich, D. Q. (2019). Changes in the acute
747 response of respiratory diseases to PM 2.5 in New York State from 2005 to
748 2016. *Science of the Total Environment*, 677, 328-339.
749 <https://doi.org/10.1016/j.scitotenv.2019.04.357>

750 Hu, J., Chen, J., Ying, Q., & Zhang, H. (2016). One-year simulation of ozone and
751 particulate matter in China using WRF/CMAQ modeling system. *Atmospheric*
752 *Chemistry and Physics*, 16(16), 10333-10350. [https://doi.org/10.5194/acp-16-](https://doi.org/10.5194/acp-16-10333-2016)
753 [10333-2016](https://doi.org/10.5194/acp-16-10333-2016)

754 Hu, J., Wu, L., Zheng, B., Zhang, Q., He, K., Chang, Q., Li, X., Yang, F., Ying, Q., &
755 Zhang, H. (2015). Source contributions and regional transport of primary
756 particulate matter in China. *Environmental Pollution*, 207, 31-42.
757 <https://doi.org/10.1016/j.envpol.2015.08.037>

758 Hua, J., Zhang, Y., de Foy, B., Shang, J., Schauer, J. J., Mei, X., Sulaymon, I. D., & Han,
759 T. (2021). Quantitative estimation of meteorological impacts and the COVID-
760 19 lockdown reductions on NO₂ and PM_{2.5} over the Beijing area using
761 Generalized Additive Models (GAM). *Journal of Environmental Management*,
762 291. <https://doi.org/10.1016/j.jenvman.2021.112676>

763 Huang, J.P., Fung, J.C.H., Lau, A.K.H., & Qin, Y. (2005). Numerical Simulation and
764 Process Analysis of Typhoon-Related Ozone Episodes in Hong Kong, p. 110.

765 Jiang, Y., Xing, J., Wang, S., Chang, X., Liu, S., Shi, A., Liu, B., & Sahu, S. K. (2021).
766 Understand the local and regional contributions on air pollution from the view of
767 human health impacts. *Frontiers of Environmental Science and Engineering*, 15(5).
768 <https://doi.org/10.1007/s11783-020-1382-2>

769 Kwok, R. H. F., Napelenok, S. L., & Baker, K. R. (2013). Implementation and evaluation
770 of PM_{2.5} source contribution analysis in a photochemical model. *Atmospheric*
771 *Environment*, 80, 398-407. <https://doi.org/10.1016/j.atmosenv.2013.08.017>

772 Li, L., Chen, C.H., Huang, C., Huang, H.Y., Zhang, G.F., Wang, Y.J., Wang, H.L., Lou,
773 S.R., Qiao, L.P., Zhou, M., Chen, M.H., Chen, Y.R., Streets, D.G., Fu, J.S., & Jang,
774 C.J. (2012). Process analysis of regional ozone formation over the Yangtze River
775 Delta, China using the Community Multi-scale Air Quality modeling system.
776 *Atmos. Chem. Phys.* 12, 10971-10987.

777 Li, L., Li, Q., Huang, L., Wang, Q., Zhu, A., Xu, J., Liu, Z., Li, H., Shi, L., Li, R., Azari,
778 M., Wang, Y., Zhang, X., Liu, Z., Zhu, Y., Zhang, K., Xue, S., Ooi, M. C. G.,
779 Zhang, D., & Chan, A. (2020). Air quality changes during the COVID-19 lockdown
780 over the Yangtze River Delta Region: An insight into the impact of human
781 activity pattern changes on air pollution variation. *Science of the Total*
782 *Environment*, 732. <https://doi.org/10.1016/j.scitotenv.2020.139282>

783 Li, M., Song, Y., Huang, X., Li, J., Mao, Y., Zhu, T., Cai, X., & Liu, B. (2014). Improving
784 mesoscale modeling using satellite-derived land surface parameters in the Pearl
785 River Delta region, China. *Journal of Geophysical Research*, 119(11), 6325-6346.
786 <https://doi.org/10.1002/2014JD021871>

787 Li, M., Zhang, Z., Yao, Q., Wang, T., Xie, M., Li, S., Zhuang, B., & Han, Y. (2021).
788 Nonlinear responses of particulate nitrate to NO_x emission controls in the
789 megalopolises of China. *Atmospheric Chemistry and Physics*, 21(19), 15135-
790 15152. <https://doi.org/10.5194/acp-21-15135-2021>

791 Li, X., Huang, L., Li, J., Shi, Z., Wang, Y., Zhang, H., Ying, Q., Yu, X., Liao, H., & Hu,
792 J. (2019). Source contributions to poor atmospheric visibility in China.
793 *Resources, Conservation & Recycling*, 143: 167-177.

794 Liu, J., Mauzerall, D. L., Chen, Q., Zhang, Q., Song, Y., Peng, W., Klimont, Z., Qiu, X.
795 H., Zhang, S. Q., Hu, M., Lin, W. L., Smith, K. R., & Zhu, T. (2016) Air
796 pollutant emissions from Chinese households: A major and underappreciated
797 ambient pollution source. *P. Natl. Acad. Sci. USA*, 113, 7756-7761.

798 Liu, P., & Zhang, Y. (2011). Use of a process analysis tool for diagnostic study on fine
799 particulate matter predictions in the U.S. Part II: analyses and sensitivity
800 simulations. *Atmos. Poll. Res.* 2, 61-71.

801 Liu, T., Wang, X., Hu, J., Wang, Q., An, J., Gong, K., Sun, J., Li, L., Qin, M., Li, J., Tian,
802 J., Huang, Y., Liao, H., Zhou, M., Hu, Q., Yan, R., Wang, H., & Huang, C. (2020).
803 Driving Forces of Changes in Air Quality during the COVID-19 Lockdown Period
804 in the Yangtze River Delta Region, China. *Environmental Science and Technology*
805 *Letters*, 7(11), 779-786. <https://doi.org/10.1021/acs.estlett.0c00511>

806 Liu, X.H., Zhang, Y., Xing, J., Zhang, Q., Wang, K., Streets, D.G., Jang, C., Wang,
807 W.X., & Hao, J.M. (2010). Understanding of regional air pollution over China
808 using CMAQ. Part II: process analysis and sensitivity of ozone and particulate
809 matter to precursor emissions. *Atmos. Environ.* 44, 3719-3727.

810 Ma, J., Shen, J., Wang, P., Zhu, S., Wang, Y., Wang, P., Wang, G., Chen, J., & Zhang, H.
811 (2021). Modeled changes in source contributions of particulate matter during the
812 COVID-19 pandemic in the Yangtze River Delta, China. *Atmospheric Chemistry*
813 *and Physics*, 21(9), 7343-7355. <https://doi.org/10.5194/acp-21-7343-2021>

814 Mishra, R., Mishra, N.C., Singh, R., & Mishra, R. (2021). Improvement of atmospheric
815 pollution in the capital cities of US during COVID-19,
816 <https://doi.org/10.1002/essoar.10505250.2>

817 Muhammad, S., Long, X., & Salman, M. (2020). COVID-19 pandemic and environmental
818 pollution: A blessing in disguise? *Science of the Total Environment*, 728.
819 <https://doi.org/10.1016/j.scitotenv.2020.138820>

820 Orak, N. H., & Ozdemir, O. (2021). The impacts of COVID-19 lockdown on PM₁₀ and
821 SO₂ concentrations and association with human mobility across Turkey.
822 *Environmental Research*, 197. <https://doi.org/10.1016/j.envres.2021.111018>.

823 Qiao, X., Tang, Y., Hu, J., Zhang, S., Li, J., Kota, S. H., Wu, L., Gao, H., Zhang, H., &
824 Ying, Q. (2015). Modeling dry and wet deposition of sulfate, nitrate, and
825 ammonium ions in Jiuzhaigou National Nature Reserve, China using a source-
826 oriented CMAQ model: Part I. Base case model results. *Science of the Total*
827 *Environment*, 532, 831-839. <https://doi.org/10.1016/j.scitotenv.2015.05.108>

828 Querol, X., Massagué, J., Alastuey, A., Moreno, T., Gangoiti, G., Mantilla, E., Duéguéz, J.
829 J., Escudero, M., Monfort, E., Pérez García-Pando, C., Petetin, H., Jorba, O.,
830 Vázquez, V., de la Rosa, J., Campos, A., Muñoz, M., Monge, S., Hervás, M., Javato,
831 R., & Cornide, M. J. (2021). Lessons from the COVID-19 air pollution decrease in
832 Spain: Now what? *Science of the Total Environment*, 779.
833 <https://doi.org/10.1016/j.scitotenv.2021.146380>

834 Shang, X., Zhang, K., Meng, F., Wang, S., Lee, M., Suh, I., Kim, D., Jeon, K., Park, H.,
835 Wang, X., & Zhao, Y. (2018). Characteristics and source apportionment of fine
836 haze aerosol in Beijing during the winter of 2013. *Atmospheric Chemistry and*
837 *Physics*, 18(4), 2573-2584. <https://doi.org/10.5194/acp-18-2573-2018>

838 Sharma, S., Zhang, M., Anshika, Gao, J., Zhang, H., & Kota, S. H. (2020). Effect of
839 restricted emissions during COVID-19 on air quality in India. *Science of the*
840 *Total Environment*, 728. <https://doi.org/10.1016/j.scitotenv.2020.138878>

841 Shen, J., Zhao, Q., Cheng, Z., Huo, J., Zhu, W., Zhang, Y., Duan, Y., Wang, X., Antony
842 Chen, L. W., & Fu, Q. (2020). Evolution of source contributions during heavy fine
843 particulate matter (PM_{2.5}) pollution episodes in eastern China through online
844 measurements. *Atmospheric Environment*, 232.
845 <https://doi.org/10.1016/j.atmosenv.2020.117569>

846 Shen, L., Wang, H., Zhu, B., Zhao, T., Liu, A., Lu, W., Kang, H., & Wang, Y. (2021).
847 Impact of urbanization on air quality in the Yangtze River Delta during the
848 COVID-19 lockdown in China. *Journal of Cleaner Production*, 296.
849 <https://doi.org/10.1016/j.jclepro.2021.126561>

850 Shen, L., Zhao, T., Wang, H., Liu, J., Bai, Y., Kong, S., Zheng, H., Zhu, Y., & Shu, Z.
851 (2021). Importance of meteorology in air pollution events during the city
852 lockdown for COVID-19 in Hubei Province, Central China. *Science of the Total*
853 *Environment*, 754. <https://doi.org/10.1016/j.scitotenv.2020.142227>

854 Shi, Z., Huang, L., Li, J., Ying, Q., Zhang, H., & Hu, J. (2020). Sensitivity analysis of the
855 surface ozone and fine particulate matter to meteorological parameters in China.
856 *Atmospheric Chemistry and Physics*, 20(21), 13455-13466.
857 <https://doi.org/10.5194/acp-20-13455-2020>

858 Shi, Z., Li, J., Huang, L., Wang, P., Wu, L., Ying, Q., Zhang, H., Lu, L., Liu, X., Liao, H.,
859 & Hu, J. (2017). Source apportionment of fine particulate matter in China in 2013
860 using a source-oriented chemical transport model. *Science of the Total*
861 *Environment*, 1476-1487. <https://doi.org/10.1016/j.scitotenv.2017.06.019>

- 862 Singh, R.P., & Chauhan, A.K. (2020). Impact of lockdown on air quality in India during
863 COVID-19 pandemic. *Air Quality, Atmosphere and Health*, Volume: 13, Issue: 8,
864 921-928.
- 865 Srivastava, A. (2021). COVID-19 and air pollution and meteorology-an intricate
866 relationship: A review. In *Chemosphere* (Vol. 263). Elsevier Ltd.
867 <https://doi.org/10.1016/j.chemosphere.2020.128297>
- 868 Sulaymon, I. D., Mei, X., Yang, S., Chen, S., Zhang, Y., Hopke, P. K., Schauer, J. J., &
869 Zhang, Y. (2020). PM_{2.5} in Abuja, Nigeria: Chemical characterization, source
870 apportionment, temporal variations, transport pathways and the health risks
871 assessment. *Atmospheric Research*, 237.
872 <https://doi.org/10.1016/j.atmosres.2019.104833>
- 873 Sulaymon, I. D., Zhang, Y., Hopke, P. K., Hu, J., Zhang, Y., Li, L., Mei, X., Gong, K., Shi,
874 Z., Zhao, B., & Zhao, F. (2021a). Persistent high PM_{2.5} pollution driven by
875 unfavorable meteorological conditions during the COVID-19 lockdown period in
876 the Beijing-Tianjin-Hebei region, China. *Environmental Research*, 198.
877 <https://doi.org/10.1016/j.envres.2021.111186>
- 878 Sulaymon, I. D., Zhang, Y., Hu, J., Hopke, P. K., Zhang, Y., Zhao, B., Xing, J., Li, L., &
879 Mei, X. (2021b). Evaluation of regional transport of PM_{2.5} during severe
880 atmospheric pollution episodes in the western Yangtze River Delta, China.
881 *Journal of Environmental Management*, 293.
882 <https://doi.org/10.1016/j.jenvman.2021.112827>
- 883 Sulaymon, I. D., Zhang, Y., Hopke, P. K., Zhang, Y., Hua, J., & Mei, X. (2021c). COVID-
884 19 pandemic in Wuhan: Ambient air quality and the relationships between criteria
885 air pollutants and meteorological variables before, during, and after lockdown.
886 *Atmospheric Research*, 250. <https://doi.org/10.1016/j.atmosres.2020.105362>
- 887 Sulaymon, I. D., Zhang, Y., Hopke, P. K., Hu, J., Rupakheti, D., Xie, X., Zhang, Y.,
888 Ajibade, F. O., Hua, J., & She, Y. (2021d). Influence of transboundary air pollution
889 and meteorology on air quality in three major cities of Anhui Province, China.
890 *Journal of Cleaner Production*, 129641.
891 <https://doi.org/10.1016/j.jclepro.2021.12964>
- 892 Sulaymon, I.D., Zhang, Y., Hopke, P.K., Guo, S., Ye, F., Sun, J., Zhu, Y., & Hu, J. (2023).
893 Quantifying the contributions of atmospheric processes and meteorology to severe
894 PM_{2.5} pollution episodes during the COVID-19 lockdown in the Beijing-Tianjin-
895 Hebei, China. [Dataset]. Zenodo. <https://doi.org/10.5281/zenodo.7711747>
- 896 Tang, L., Shang, D., Fang, X., Wu, Z., Qiu, Y., Chen, S., Li, X., Zeng, L., Guo, S., & Hu,
897 M. (2021). More significant impacts from new particle formation on haze
898 formation during COVID-19 lockdown. *Geophysical Research Letters*, 48,
899 e2020GL091591. <https://doi.org/10.1029/2020GL091591>
- 900 Wang, B., Qiu, T., & Chen, B. (2014). Photochemical process modeling and analysis of
901 ozone generation. *Chin. J. Chem. Eng.* 22, 721-729.
- 902 Wang, N., Lyu, X. P., Deng, X. J., Guo, H., Deng, T., Li, Y., Yin, C. Q., Li, F., & Wang,
903 S. Q. (2016). Assessment of regional air quality resulting from emission control
904 in the Pearl River Delta region, southern China. *Science of the Total
905 Environment*, 573, 1554-1565. <https://doi.org/10.1016/j.scitotenv.2016.09.013>
- 906 Wang, P., Chen, K., Zhu, S., Wang, P., & Zhang, H. (2020). Severe air pollution events
907 not avoided by reduced anthropogenic activities during COVID-19 outbreak.

908 Resources, Conservation and Recycling, 158.
909 <https://doi.org/10.1016/j.resconrec.2020.104814>

910 Wang, P., Ying, Q., Zhang, H., Hu, J., Lin, Y., & Mao, H. (2018). Source apportionment
911 of secondary organic aerosol in China using a regional source-oriented
912 chemical transport model and two emission inventories. *Environmental*
913 *Pollution*, 237, 756-766. <https://doi.org/10.1016/j.envpol.2017.10.122>

914 Wang, X., Li, L., Gong, K., Mao, J., Hu, J., Li, J., Liu, Z., Liao, H., Qiu, W., Yu, Y.,
915 Dong, H., Guo, S., Hu, M., Zeng, L., & Zhang, Y. (2021). Modelling air quality
916 during the EXPLORE-YRD campaign - Part I. Model performance evaluation and
917 impacts of meteorological inputs and grid resolutions. *Atmospheric Environment*,
918 246. <https://doi.org/10.1016/j.atmosenv.2020.118131>

919 Wang, X., Zhang, Y., Hu, Y., Zhou, W., Lu, K., Zhong, L., Zeng, L., Shao, M., Hu, M.,
920 & Russell, A.G. (2010). Process analysis and sensitivity study of regional ozone
921 formation over the Pearl River Delta, China, during the PRIDE-PRD2004
922 campaign using the Community Multiscale Air Quality modeling system. *Atmos.*
923 *Chem. Phys.* 10, 4423-4437.

924 Wu, C., Wang, H., Cai, W., He, H., Ni, A., & Peng, Z. (2021). Impact of the COVID-19
925 lockdown on roadside traffic related air pollution in Shanghai, China. *Building*
926 *and Environment*, 194. <https://doi.org/10.1016/j.buildenv.2021.107718>

927 Xing, J., Zhang, Y., Wang, S.X., Liu, X.H., Cheng, S.H., & Zhang, Q. (2011). Modeling
928 study on the air quality impacts from emission reductions and atypical
929 meteorological conditions during the 2008 Beijing Olympics. *Atmos. Environ.* 45,
930 1786-1798.

931 Xing, J., Li, S., Jiang, Y., Wang, S., Ding, D., Dong, Z., Zhu, Y., & Hao, J. (2020).
932 Quantifying the emission changes and associated air quality impacts during the
933 COVID-19 pandemic on the North China Plain: A response modeling study.
934 *Atmospheric Chemistry and Physics*, 20(22), 14347-14359.
935 <https://doi.org/10.5194/acp-20-14347-2020>

936 Xue, T., Liu, J., Zhang, Q., Geng, G., Zheng, Y., Tong, D., Liu, Z., Guan, D., Bo, Y., Zhu,
937 T., He, K., & Hao, J. (2019). Rapid improvement of PM_{2.5} pollution and associated
938 health benefits in China during 2013-2017. *Science China Earth Sciences*, 62(12),
939 1847-1856. <https://doi.org/10.1007/s11430-018-9348-2>

940 Xu, W., Song, W., Zhang, Y., Liu, X., Zhang, L., Zhao, Y., Liu, D., Tang, A., Yang, D.,
941 Wang, D., Wen, Z., Pan, Y., Fowler, D., Collett, J. L., Willem Erisman, J., Goulding,
942 K., Li, Y., & Zhang, F. (2017). Air quality improvement in a megacity: Implications
943 from 2015 Beijing Parade Blue pollution control actions. *Atmospheric Chemistry*
944 *and Physics*, 17(1), 31-46. <https://doi.org/10.5194/acp-17-31-2017>

945 Yan, D., Lei, Y., Shi, Y., Zhu, Q., Li, L., & Zhang, Z. (2018). Evolution of the
946 spatiotemporal pattern of PM_{2.5} concentrations in China - A case study from
947 the Beijing-Tianjin-Hebei region. *Atmospheric Environment*, 183, 225-233.
948 <https://doi.org/10.1016/j.atmosenv.2018.03.041>

949 Ye, F., Rupakheti, D., Huang, L., T, Nishanth., MK, S.K., Li, L., KT, V., & Hu, J. (2022).
950 Integrated process analysis retrieval of changes in ground-level ozone and fine
951 particulate matter during the COVID-19 outbreak in the coastal city of Kannur,
952 India. *Environmental Pollution*, 307. <https://doi.org/10.1016/j.envpol.2022.119468>

953 Yin, P., Brauer, M., Cohen, A.J., Wang, H., Li, J., Burnett, R.T., Stanaway, J.D., Causey,
954 K., Larson, S., Godwin, W., Frostad, J., Marks, A., Wang, L., Zhou, M., & Murray,
955 C.J.L. (2020). The effect of air pollution on deaths, disease burden, and life
956 expectancy across China and its provinces, 1990-2017: an analysis for the Global
957 Burden of Disease Study 2017. *The Lancet Planetary Health* 4, e386–e398.

958 Zhang, Y., Ma, Z., Gao, Y., & Zhang, M. (2021). Impacts of the meteorological condition
959 versus emissions reduction on the PM_{2.5} concentration over Beijing-Tianjin-Hebei
960 during the COVID-19 lockdown. *Atmospheric and Oceanic Science Letters*, 14(4).
961 <https://doi.org/10.1016/j.aosl.2020.100014>

962 Zhao, N., Wang, G., Li, G., Lang, J., & Zhang, H. (2020). Air pollution episodes during
963 the COVID-19 outbreak in the Beijing-Tianjin-Hebei region of China: An insight
964 into the transport pathways and source distribution. *Environmental Pollution*, 267.
965 <https://doi.org/10.1016/j.envpol.2020.115617>

966 Zhao, X., Wang, G., Wang, S., Zhao, N., Zhang, M., & Yue, W. (2021). Impacts of
967 COVID-19 on air quality in mid-eastern China: An insight into meteorology
968 and emissions. *Atmospheric Environment*, 266.
969 <https://doi.org/10.1016/j.atmosenv.2021.118750>

970 Zheng, B., Zhang, Q., Geng, G., Chen, C., Shi, Q., Cui, M., Lei, Y., & He, K. (2021).
971 Changes in China's anthropogenic emissions and air quality during the
972 COVID-19 pandemic in 2020. *Earth System Science Data*, 13(6), 2895-2907.
973 <https://doi.org/10.5194/essd-13-2895-2021>

974 Zheng, B., Zhang, Q., Geng, G., Shi, Q., Lei, Y., & He, K. (2020). Changes in China's
975 anthropogenic emissions during the COVID-19 pandemic. *Earth System Science*
976 *Data Discussions*, 1-20. <https://doi.org/10.5194/essd-2020-355>

977 Zhou, C., Zhou, H., Holsen, T. M., Hopke, P. K., Edgerton, E. S., & Schwab, J. J. (2019).
978 Ambient Ammonia Concentrations Across New York State. *Journal of Geophysical*
979 *Research: Atmospheres*, 124(14), 8287-8302.
980 <https://doi.org/10.1029/2019JD030380>

981 Zhu, N., Zhang, D., Wang, W., Li, X., Yang, B., Song, J., Zhao, X., Huang, B., Shi, W.,
982 Lu, R., Niu, P., Zhan, F., Ma, X., Wang, D., Xu, W., Wu, G., Gao, G. F., & Tan,
983 W. (2020). A Novel Coronavirus from Patients with Pneumonia in China, 2019.
984 *New England Journal of Medicine*, 382(8), 727-733.
985 <https://doi.org/10.1056/nejmoa2001017>